

## Review

## A review of microfluidic-based mixing methods



Zhenghua Li<sup>a,1</sup>, Baoliang Zhang<sup>a,1</sup>, Dan Dang<sup>b,\*</sup>, Xieliu Yang<sup>a</sup>, Wenguang Yang<sup>c</sup>,  
Wenfeng Liang<sup>a,\*2</sup>

<sup>a</sup> School of Mechanical Engineering, Shenyang Jianzhu University, Shenyang 110168, China

<sup>b</sup> School of Sciences, Shenyang Jianzhu University, Shenyang 110168, China

<sup>c</sup> School of Electromechanical and Automotive Engineering, Yantai University, Yantai 264005, China

## ARTICLE INFO

**Keywords:**  
Microfluidic device  
Mixing  
Active method  
Passive method

## ABSTRACT

Microfluidic-based mixing methods have aroused increasing attention due to their tremendous potential in bio-related and materials science fields. Achieving mixing based on microscale devices, microfluidic-based mixing methods offer several advantages over their macroscale device-based counterparts, such as compact size, ease of operation, and the straightforward control of the mixing process. Generally, the ability to achieve high mixing performance in an efficient and simple manner is a key criterion for the reliability of a microfluidic-based method, which is essential to the reactor design. In the review paper, we summarize a number of microfluidic-based mixing methods capable of synthesizing nanoparticles. For comparative purposes, we divide these methods into active and passive methods, looking at their working principles as well as their respective advantages. On this basis, we present five commonly used active methods and three representative passive methods, with a detailed discussion on the practical applications of each method in improving the performance of fluid mixing. At the end of the review, we elaborate on some of current limitations and future prospects of these methods, which will help guide readers who are interested in making some innovations in this area of research.

## 1. Introduction

Microfluidics has been developing for decades due to their wide range of applications. This technique can treat fluids in devices with a dimension ranging from hundreds of micrometers to a few millimeters [1]. Microfluidic-based mixing is one of the most common operations and applications in the microfluidic field. Micro-mixing refers specifically to mixing two or more types of fluids together uniformly in a microscale microfluidic chip [2]. Nowadays, it is widely used in a series of fields such as chemistry [3], biology [4], clinical diagnosis [5], drug development [6], and materials science [7]. For example, micromixer devices can be used to synthesize silicon nanoparticles using the Stöber method, which the size distribution of particles is narrow due to the extremely homogeneous mixed solutions [8]. Micromixer methods can also be used to synthesize extremely homogeneous layered Ni-rich cathode materials to help improve the electrochemical performance of batteries significantly [9]; microfluidic devices can reduce the reaction

time of reactants from 12 h to several seconds. Furthermore, micromixer methods can mix samples efficiently and precisely, which ensures the integrity of samples and proper distribution of proteins that are critical to determining the structures of biological macromolecules to investigate biological functions [10]. Moreover, micromixer chips can mix samples with enzyme and thereby detect the concentration of excessive pesticide residues in food with much reduced costs and higher sensitivity [11]. In addition, micromixer chips also offer efficient way to prevent drugs from aggregating and improve their absorption in the body by coating the drug with a substance, such as lipid [12]. Recent advances in microfabrication, such as soft lithography and 3D printing, have opened up new capabilities for the application of micromixing devices. In this context, we have seen a growing number of creative ideas on how to achieve high mixing performance with improved efficiency and operability [13]. For example, a three-layer microfluidics reaction chip was developed to flow and mix two fluids by controlling gas extrusion in the upper chamber [14]. The width of the channel

\* Corresponding authors.

E-mail addresses: [dangdan@sjzu.edu.cn](mailto:dangdan@sjzu.edu.cn) (D. Dang), [liangwf@sjzu.edu.cn](mailto:liangwf@sjzu.edu.cn) (W. Liang).

<sup>1</sup> These two authors contributed equally to this paper.

<sup>2</sup> ORCID: 0000-0002-6605-2511

shrank from 5000–300  $\mu\text{m}$ , and a floating block was set in the fluidic channel to prevent generation of backflow. In addition, a method that uses injection molded plastics for large-scale manufacture of chips was proposed [15]. The advantage of this method is that no error occurs in the large-scale manufacture of high-precision chips.

The most prominent application of microfluidic mixing is the chemical reaction between reactants. A rapidly and controllably created homogeneous reactant mixture can dramatically improve the chemistry of the end results. For example, the size distribution of nanoparticles synthesized by a micromixer chip can be decreased significantly due to more ideal mixing performance [16]. Synthesis of nanoparticles by microfluidic mixing has several important advantages. For example, the reaction process can be controlled precisely to meet the strict requirements of some sophisticated experiments; reaction conditions can be flexibly changed to suit different reactant requirements; the small batch-to-batch variations permit better repeatability of the chip [17]. Owing to the above-mentioned advantages, nanoparticles synthesized in micromixers have some unique features in terms of size [18], surface [19], chemical [20] and physical properties [21]. For example, Wu et al. used nanoparticles with a porous structure to attach small groups of  $\text{Fe}_3\text{O}_4$  nanoparticles to the surface, which allowed the drug loaded nanoparticles to be driven magnetically and move following a defined path [22]. In addition, researchers around the world have been working to develop microfluidic-based mechanisms for the synthesis of different types of nanoparticles, such as hydrophobic nanoparticles with a multi-layer structure [23], silicon nanoparticles with drug loading functions [24], and magnetic nanoparticles capable of directional motion [25]. These multifunctional nanoparticles can be used in various fields to facilitate the actual production process. For example, poly (lactide-co-glycolide)-b-poly(ethylene glycol) (PLGA-PEG) nanoparticles is a representative multi-layer structure. Specifically, PLGA provides a biocompatible and biodegradable matrix for encapsulation and release of drugs, and PEG makes the drugs stay in blood for longer periods of time [26]. In addition, the hydrophilic PEG can be protected by the hydrophobicity of PLGA, which helps to solve problems with drug adsorption and aggregation. Another straightforward application of microfluidic mixing is the precise control of the concentration of fluids. For example, Zhang's research group developed a device that utilized passive methods to mix fluids in an ultra-long-range linear concentration gradient [27]. In contrast to traditional devices, this device overcomes the limitation that only one concentration can be produced. Finally, they used these different concentrations of droplets to verify that different levels of cancer cells show different levels of drug resistance.

Flow fluctuation is an important phenomenon reflecting the rapid mixing of fluids [28]. Furthermore, the fluids with a lower Renault ( $Re$ ) rely primarily on molecular diffusion, and those with a higher  $Re$  rely primarily on chaotic vortex [29]. Micro-mixing is a concept that induces fluids to mix rapidly by breaking up the slow diffusion between molecules, which is not limited by other conditions, such as  $Re$  [30]. Micro-mixing methods can be divided into active and passive mixing methods depending on whether any external energy is added to assist with fluid mixing. Generally, the external energies utilized in active methods include magnetism [31], acoustics [32], and electricity [33]. All these energies are used to disturb fluids and create a chaotic flow, and the mixing efficiency is greatly improved due to an increased contact area between fluids. Active methods have several remarkable advantages. On the one hand, these methods can control the mixing process with higher performance. On the other hand, they allow for flexible selection of parameters to apply a variety of experimental requirements. However, these advantages represent a high requirement for operating skills and more complex structures. Passive methods utilize the vortex created when the fluids flow against some obstacles to improve the mixing efficiency, which increases the flow length of the fluids and introduces fluid disturbances in the channel [34]. These methods rely primarily on structural innovation for improving the

mixing efficiency. In terms of their advantages, these methods have a lower requirement for operating skills and a simple chip structure, and the degree of mixing is determined only by the device configuration and manual control of the flow rate. Generally, active methods have higher mixing efficiency compared with passive methods and time-pulsing flow caused by a periodical change of external energies. Therefore, active methods have more applications, such as droplet-based mixing [35], time-dependent mixing [36], and multi-steps mixing [37]. In contrast, passive micromixers have been widely used in microfluidic devices due to their easy fabrication and easy integration into microdevices, especially their minimal impact on samples. Consequently, passive mixers are a popular choice in chemical [38] and biological [10] microfluidics. Several methods have been proposed to meet higher production requirements, such as low-cost device fabrication, high mixing performance, and ease of operation [39]. All these criteria are used to determine the reliability and efficiency of a microfluidic mixing chip.

The final mixing degree is the sole criterion for the reliability of these methods. The mixing index calculated at the outlet is a key math criterion to measure the mixing degree of fluids. The most common formula for calculating the mixing index is to show the mixing degree by utilizing the difference in the grayscale value of pixel intensity between the inlet and outlet [40–42]. Firstly, the microscope image is converted to grayscale image, and then the pixel grayscale intensity value at each width cross section of the inlet and outlet is extracted through image processing. The collected data is converted into a mixing index after calculation by a set of formula. The details are shown as follows:

$$\sigma^2 = \frac{1}{n} \sum_{i=1}^n (I_i - I_m)^2 \quad (1)$$

where  $n$  is the number of pixels in the cross section,  $I_i$  is the grayscale value of pixel intensity,  $I_m$  is the mean of the grayscale values of pixel intensity of  $n$  pixels, and  $\sigma$  is the standard deviation of the intensity distribution across the width of the outlet cross section.

$$M = 1 - \frac{\sigma}{\sigma_0} \quad (2)$$

where  $M$  is the mixing degree ranging from 0 to 1, and  $\sigma_0$  is the standard deviation at the inlet cross section. As we have learnt from a comprehensive review of the existing literature, a method is reliable only when the mixing index of the outlet is greater than 90%. The mixing degree is directly correlated with the reaction rate, namely, a higher mixing index means better reaction results [43].

Micro-mixing methods for mixing two or more fluids in a microfluidic chip have been reviewed elsewhere. Some reviews analyzed the advantages and disadvantages of various micro-mixing methods by summarizing their applications, such as nanoparticle synthesis [44], chemical synthesis [45], and biomedical research [44]. In addition, there also have been reviews focusing on the mixing methods alone [40, 46, 47]. Nonetheless, there is still a lack of systematic reviews on fluid mixing methods, especially on researches published in the past five years. In view of this, we present here a comprehensive review on fluid mixing methods based on passive and active devices. We start with a look at the working principle of active methods (magnetism, acoustics, electricity, and heat) and passive methods. Then, we provide examples to explain how each method mixes fluids inside the microchannel and a comparison of the advantages and disadvantages of each method. Finally, we discuss the future developments of micromixing techniques.

## 2. Active methods

Active methods can increase the contact area between fluids to improve the mixing efficiency by adding external energies that can disturb fluids to produce a chaotic flow. In these schemes, magnetic-based micromixer relies on rotating steel balls within the channel to achieve mixing. Acoustic-based micromixer transmit acoustic energy

into a fluid medium and induce mixing through acoustic waves or acoustically vibrating microstructures. Electric-based micromixer make use of the different electrical properties between two fluids and creates transversal secondary flow by AC electrical fields. In particular, these methods can control the process or degree of mixing directly by adjusting the magnitude of these energies, and they are adaptable to many complex fields. All of these active methods expand the use of mixing in many applications, such as droplet-based mixing, multiple samples and time-dependent mixing. These energies include magnetism, acoustics, electricity, heat and so on. The working principles of these methods are detailed as follows.

## 2.1. Magnetic field

Magnetically driven micro-scale mixers are mainly available in magnetic hydrodynamics and magnetic stirring techniques (Table 1). Lorentz forces are applied to a magnetic fluid using an external magnetic field generated by permanent magnets, direct current (DC) or alternating current (AC), which induces the stirring and mixing of secondary flow [48–52]. Micro-magnetic beads, magnetic chains, and magnetic cilia are among the mostly used to stir fluids for mixing [53–58]. The effects of magnetic field intensity, volumetric flow rate, and particle mass fraction on the length and efficiency of the mixing channel are essential factors to evaluate the reliability and efficiency of a structure. Nouri et al. performed numerical simulation by COMSOL computational software to investigate these factors and then compared the simulation results with the experimental results [59]. Improving the mixing performance and shortening the mixing length are the two ultimate goals of adjusting these three parameters. According to the final results of the experiment and simulation, these goals can be achieved by increasing the magnetic field intensity, decreasing the flow rate, and increasing the particle mass fraction.

The rotating magnetic field disturbs the normal flow of the magnetic fluid and induces the phenomenon of mixing [60]. An active mixer employing a hybrid gradient magnetic field based on magnetic actuation technology was developed to achieve several times higher mixing efficiency with reduced heat and fabrication costs of microfluidic systems [61]. Micromagnets were embedded in the bottom of the T-shaped microchannel to generate a static gradient magnetic field, and an electromagnetic coil was connected with time-varying current to generate an alternating uniform magnetic field to increase the magnetic field strength. As a result, the vibration amplitude of the microfluid in the microchannel increased by several times. This mixing system can achieve 97–99% mixing efficiency of two fluids under certain conditions without changing the micromagnet application current and the microfluidic system preparation process. Hejazian et al. proposed an idea that utilizes magnetofluidic transport to produce a pressure-driven

hydrodynamic flow [51]. First, a non-magnetic stream and a superparamagnetic stream were introduced to a linear microchannel. Then, a permanent magnet placed next to the microchannel provided a non-uniform magnetic field. The mismatching magnetic field gradients and the different levels of magnetic susceptibility between the two streams created a body force that induced fast and efficient mixing. The mixing efficiency of this device reached 88% at a flow rate of 45  $\mu\text{L}/\text{min}$ . This idea can potentially be used in a range of microfluidic devices, but its limitation in creating ferromagnetic fluids may have a severe impact on some biological or chemical solutions. Zhou et al. developed a similar structure based on a micromagnet fabricated with the mixture of neodymium (NdFeB) and polydimethylsiloxane (PDMS), instead of a permanent magnet. The micromagnet was placed 150  $\mu\text{m}$  away from the mixing channel, as shown in Fig. 1 [62]. The results showed that the micromagnet generated relatively strong magnetic forces and enabled rapid mixing. The group investigated the effect of the concentration of ferromagnetic fluid and the mass ratio of the micromagnet on the mixing performance. It was found that a smaller total flow rate would result in a longer time for the micromagnet to act on the magnetic fluid and thereby induce more adequate mixing. Their follow-up study revealed that when the magnetic bar was placed directly underneath the mixing channel and tilted at a certain angle, the magnetic fluid would accelerate as it approached the magnet and decelerate after it flowed through the magnet [63]. Placing the magnet underneath the microfluidic channel can shorten the distance between ferrofluids and the magnet. In particular, the bigger angle at which the magnet was tilted, the shorter such distance and the greater the mixing efficiency. The results showed that the best mixing performance was achieved when the magnet was tilted at an angle of 15° and 250  $\mu\text{m}$  in width. Similarly, the micromagnet made by mixing NdFeB and PDMS were placed underneath the microfluidic channel and perpendicular to the flow direction, as shown in Fig. 2 [64]. This device could generate a magnetic field for rapid mixing of superparamagnetic ferromagnetic fluids with the water flow. The micromagnets in the ferromagnetic fluid region produced a steep slope in the inverse magnetic force when the  $\text{Re}$  of fluids was less than 1, which led to a lateral/diffusive pressure gradient from the local pressure source and activated the momentum transfer between the fluids. This phenomenon induced high local mixing efficiency and a small footprint of ferromagnetic fluids. Therefore, an integrated parallel system consisting of multiple microfluidic channels and micromagnets holds great potential for rapid mixing of high flux fluids.

Cilia are a tiny, highly elastic material with magnetic properties. A typical application of cilia in fabricating micromixing systems is micromixers based on ultra-high aspect-ratio rare-earth magnetic composite polymer artificial cilia [58]. Liu et al. employed a method that prepared artificial cilia based on disperse micro-Fe particles in the PDMS matrix and made it easier and more efficient to drive cilia magnetically [65]. As shown in Fig. 3, unlike previous micro hybridized devices prepared in a complex procedure, the micro hybridized cilia in this method are prepared outside the lab-on-chip (LOC) device and then assembled with a LOC chip. In particular, hanging the cilia inside the chamber from top to down allows the cilia to respond faster to magnetism. According to comparison, the mixing performance of this structure is up to nine times better than that of diffusion mixing, especially when the electromagnet is driven by a square wave. However, the circular conical motion of artificial cilia would induce the backflow and flow oscillations and weaken the mixing performance. To address this issue, the concept of the triangular beating pattern, as shown in Fig. 4, was proposed to reduce the back flow and increase the net flow during the restoration of cilia [66]. The power supplies of four magnetic coils were connected individually and their duty cycles were altered in a range of 0–100% to produce a non-uniform and cyclically varying magnetic field. In this way, the cilia tip can traverse the desired triangular actuation path. The number of artificial cilia was set to 20 to ensure the best efficiency and prevent the asynchronous movement of cilia outside the magnetic field from obstructing the movement of fluids.

**Table 1**  
Mixing performance of magnetic-based micromixer.

Categories	Mixing technique	Mixing index	Reference
Magnetic fluid	Time-varying magnetic field intensity	99%	[61]
	Permanent magnet	88%	[51]
	NdFeB–PDMS micromagnets were placed next to the microfluidic channel	–	[62]
	NdFeB–PDMS micromagnets were placed underneath the microfluidic channel	≈ 99%	[64]
Magnetic cilia	Artificial cilia	80%	[65]
	Artificial cilia with triangular beating pattern	–	[66]
Micro-magnetic beads	Magnetic particle swarming	–	[67]
Magnetic bars	Micromagnetic bar moved in the shape of a kayak paddle	–	[30]

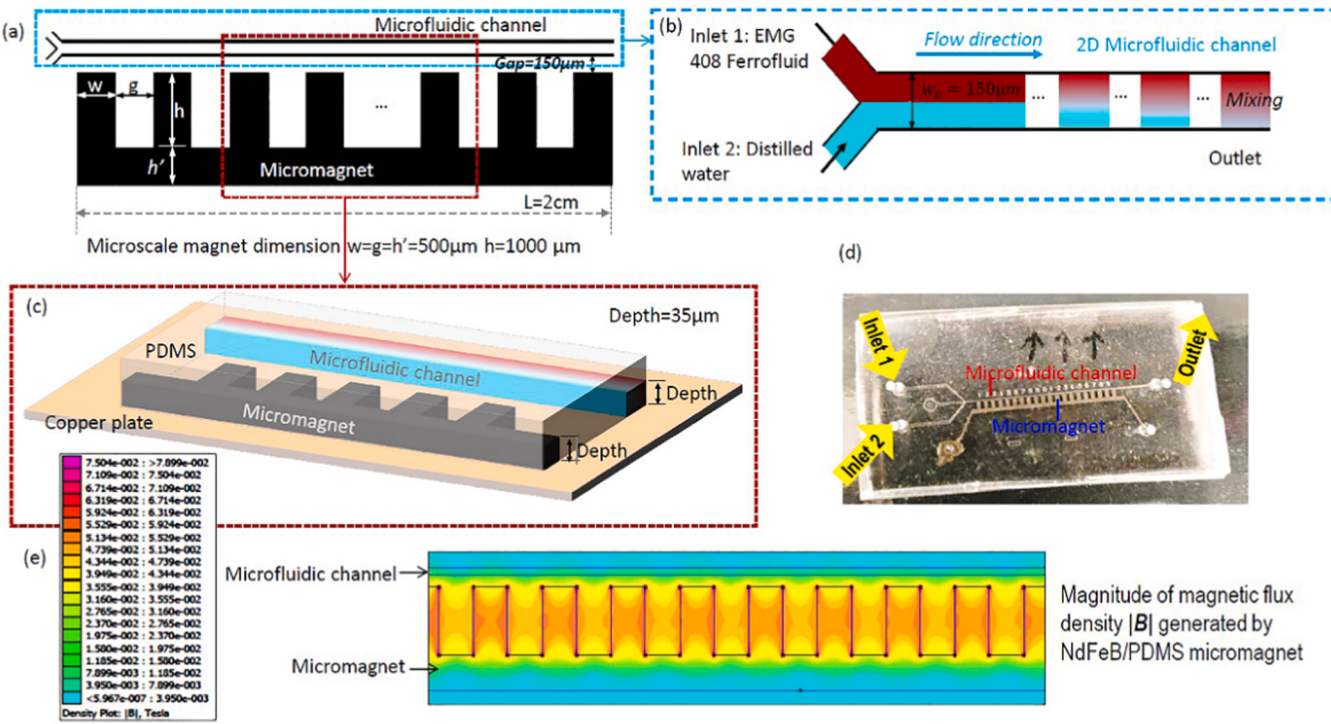


**Fig. 1.** Schematic of a rapid mixing microdevice with an embedded micromagnet. (a) The two-dimensional view of the microfluidic channel and the micromagnet. The microscale magnet is fabricated beside the microfluidic channel, and the distance between the micromagnet and the microfluidic channel is gap = 150  $\mu\text{m}$ . The width, length, and gap of the micromagnet range from 500  $\mu\text{m}$  to 1000  $\mu\text{m}$ . (b) The enlarged sketch of the microfluidic channel. The microfluidic channel has a width of  $w_c = 150\text{ }\mu\text{m}$  and both the micromagnet and microfluidic channel have a length of  $L = 2\text{ cm}$ . Inlet 1 is injected with ferrofluids and Inlet 2 is injected with distilled water. (c) The three-dimensional (3D) view of the sectional microdevice. Both the microfluidic channel and micromagnet have a depth of = 35  $\mu\text{m}$ , which is the same as the thickness of the dry photoresist film. (d) The prototype of a microfluidic device for magnetic rapid mixing. (e) The simulated contour of the magnitude of magnetic flux density  $|\mathbf{B}|$  generated by NdFeB/PDMS micromagnet [62].

Because of the smaller backflow and fluctuation, the peak rate of the net flow in the triangular hopping case was almost twice as high as that in the circular hopping case.

Previous studies have shown that the dipole-dipole interactions between magnetic beads allow suspended magnetic beads to be self-assembled into the anisotropic chains of magnetic beads under the action of an external magnetic field [57]. When these bead chains are subjected to a rotating magnetic field, they would produce a rotational motion that locally stirs and mixes the fluids (micromixer). In addition, the microfluidic mixing induced by the magnetic particle swarming (MPS) phenomenon shows potential for application in point-of-care (PoC) tests, especially for some static fluids. The most significant advantage of MPS is that the magnetic bead chains in the chamber experience both local rotational motions and global rotational motions. Therefore, Toonder et al. systematically investigated the two determinants for the occurrence of MPS, including magnetic field rotation frequency and magnetic field strength [67]. The dynamics of the magnetic particles were examined to quantify the induced fluid flow and the resulting mixing performance, such as the degree of solution mixing. As shown in Fig. 5, they created a 3D manipulation of magnetic particles by arranging two sets of electric poles on the vertical and horizontal planes, respectively. MPS enhanced the mixing process in microfluidic reaction chambers by introducing strong fluid disturbances. In particular, the operability of micro reaction chambers can be improved by this method, thereby improving the homogeneity of the initial stagnated samples in the microfluidic reaction chamber. In biomedical applications, magnetic particle mixing techniques can enable much faster detection of antibodies by bioluminescent PoC assays than non-driven diffusion-only techniques. Therefore, MPS makes the slow diffusion of water-like mixtures more general by introducing a simple technique to induce global mixing.

In contrast to ferrofluids containing high concentrations of magnetic nanoparticles, magnetic bars containing such nanoparticles can enhance the mixing performance and decrease the influence of nanoparticles on the samples. A magnetic bar-based micromixer is similarly miniaturized to the magnetic stirring bar used in macroscopic mixing operations for microfluidic devices [30]. Using a rotating magnetic field, the microbar is made to rotate in the fluid system, enhancing the mixing near the bar. In addition, a micromixer in which magnetic micropillars are arranged in an array directly at the bottom of the channel [68]. When an external magnetic field is applied to the micromixer channel, the magnetic micropillar array is attracted to one side. This method makes part of the fluid flow laterally while the micropillar moves, thus producing a mixing effect. Furthermore, a micromagnetic rod that moves in a micromixer in the shape of a kayak paddle was proposed [30]. This rod was synthesized by the sequential electrodeposition of Au-Ni-Au, and the nickel segment was tilted by  $5.4^\circ \pm 2.4^\circ$  with respect to the short axis of the rod, as shown in Fig. 6. Due to the repulsive forces between rods and the negatively charged glass floor, microbars would be suspended in the surface of the floor. While the external magnetic field was rotating, the rod produced rotational motion and at the same time precession by an angle of  $\theta$  around the y-axis, as shown in Fig. 6c. The micromagnetic rod moved in the shape of a kayak paddle because the rod segment near the surface of the floor was subjected to a greater drag force than the segment farther away. Especially, this method was the first to apply a kilohertz of frequency in the magnetic field, which allowed the magnetic control of microrods to be applied to LOP mixing and other techniques. Equipping an array of micropillars on a flexible membrane and deforming the membrane by an electromagnetic force is another structural scheme [69]. As shown in Fig. 7, the microfluidic mixer structure consisted of a microfluidic part, a mechanical part, and an electromagnetic part. The two different solution samples were injected through the

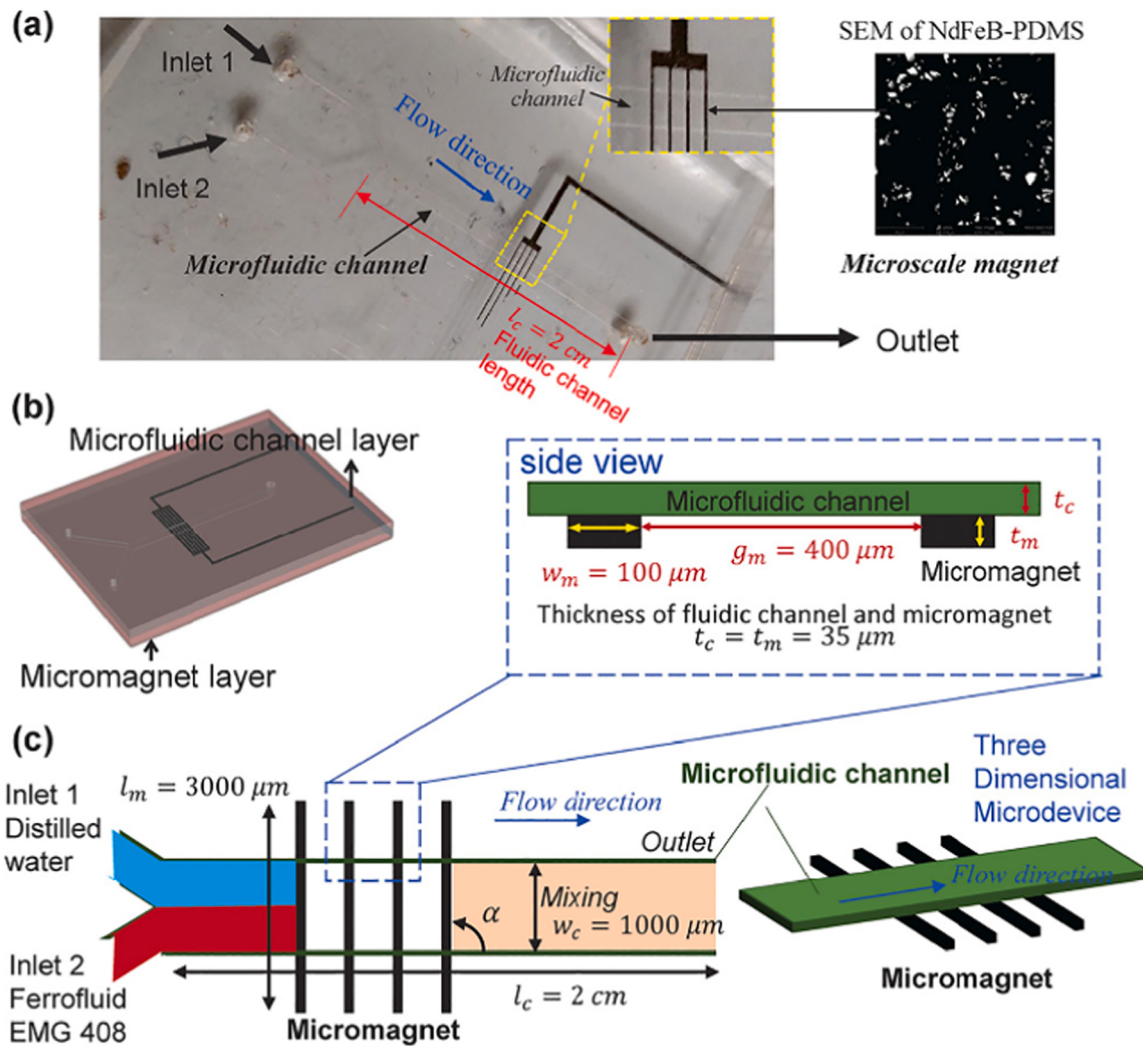


**Fig. 2.** (a) A photo of the microfluidic device for rapid mixing. The inset is the scanning electron microscopy (SEM) image of solidified NdFeB-PDMS. (b) Computer-aided design (CAD) schematic of the device. (c) Dimension description of the micromixer.  $w_c$  and  $l_c$  are the width and length of the microfluidic channel, respectively;  $\alpha = 90^\circ$  is the angle between the micromagnet and the flow direction;  $l_m$  and  $w_m$  are the length and width of each micromagnet;  $g_m$  is the gap distance between each micromagnet;  $t_m$  and  $t_c$  are the thicknesses of the microfluidic channel and the micromagnet [64].

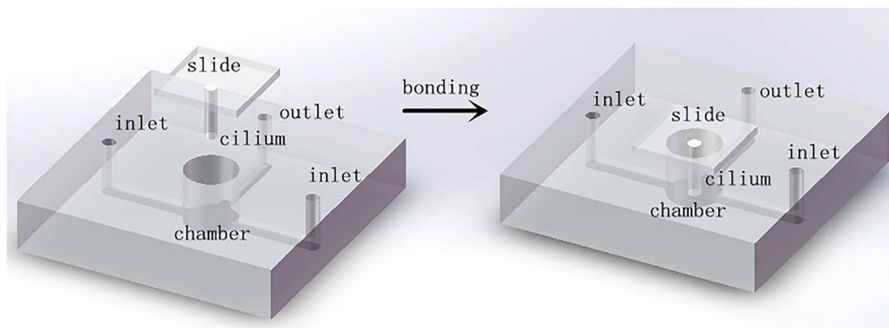


**Fig. 3.** Bonding of the fabricated cilium on the top of a mixer chamber [65].

microchannel and then mixed by the movement of micropillars on the membrane after entering the mixing chamber. All the micropillars moved upward or downward due to the membrane vibration driven by the electromagnetic part. Meanwhile, the radius and spacing of the micropillars were optimized by finite element analysis in COMSOL, and 81 micropillars were equipped on a  $4 \text{ mm}^2$  circular membrane area, which had the highest mixing degree.

The efficiency of fluid mixing inside droplets can be improved by stirring magnetic bars in the droplets [70]. These nano stir bars can create vortices inside the confined droplets, and these vortices can vigorously mix fluids without causing the droplets to destabilize or move. Furthermore, the intensity of vortices can be easily controlled by adjusting the stirring speed of the nano stir bars using the rotational magnetic field produced by a common magnetic stirrer. The mixing

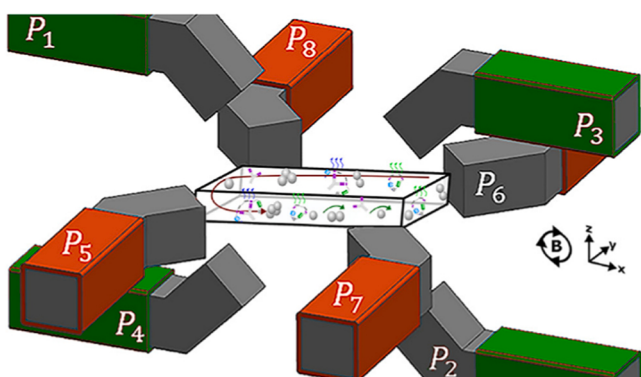
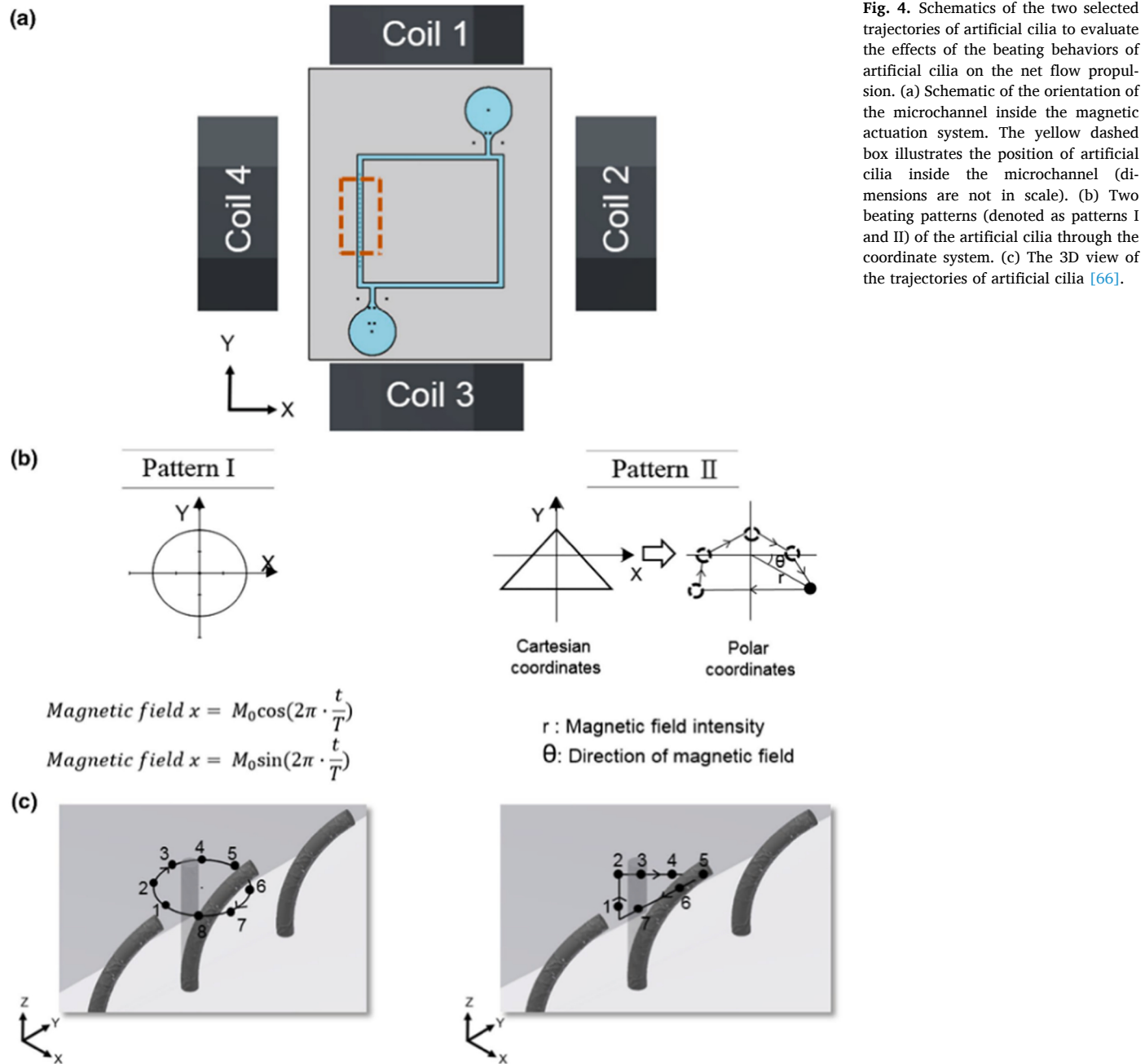


**Fig. 5.** Schematic of an octopolar electromagnetic system [67].

performance, however, does not always increase as the rotational frequency of the magnetic field increases, because the nano stir bars cannot keep up with the high rotational frequency. The mixing efficiency reaches its peak when the frequency is 20 Hz. Droplets can also be manipulated and mixed by deforming the membrane in a specialized position. Chen et al. proposed a method to mix droplets by magnetically driving droplet motion on an open surface [71]. The membrane was a super-hydrophobic and magnetically functionalized PDMS (MF-PDMS) membrane, and the surface of this membrane had an array of PDMS micropillars on it to reduce the adhesion of droplets on the surface, as shown in Fig. 8b. First, 5  $\mu$ L of droplets were placed on the membrane. Then, the membrane would produce a dent due to the gravity of the droplets. Meanwhile, the magnet was opened to control the droplets in the dent to move on a regular course. As shown in Fig. 8a, two droplets were controlled to realize coalescence and mixing by tuning the back-and-forth motion of the magnet underneath to generate the

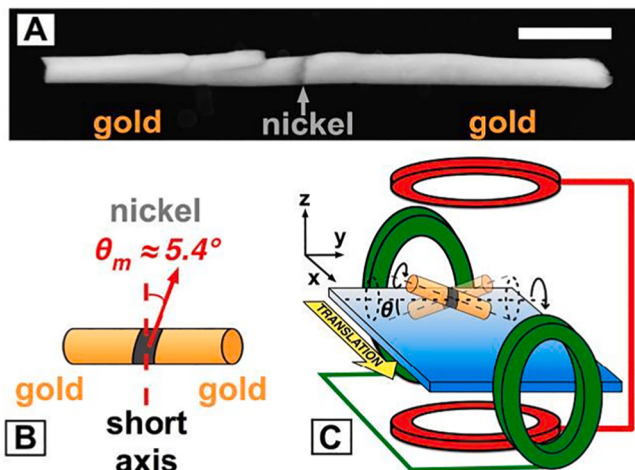


**Fig. 6.** SEM image of a rod and schematic showing rod magnetization and experimental setup. (a) An SEM image of a gold-nickel-gold rod. The nickel segment is tilted slightly around the short axis of the rod. The scale bar is  $1\text{ }\mu\text{m}$ . (b) Schematic of the rod, showing its short axis (dashed line) and magnetization angle  $\theta_m$  (indicated by the solid arrow in an enlarged view). (c) Magnetic coil arrangement, showing how rotation (around the long axis of the rod) and precession (around the y-axis) are achieved. The magnetic field orients the long axis of the rod along the y-axis (by an angle of  $\theta$ ) and rotates the rod in the xz plane. Rotation induces the translation of the rod in the X-axis. The rod precesses by an angle of  $\theta_m \approx 5.4^\circ$  [30].

internal circulations of the droplets. In addition, the platform can also be used for diluting droplets with different concentrations. The advantages of programmability, efficient mixing, and parallel scalability of this method make it suitable for use in bioanalysis, chemical microreactors, and so on.

## 2.2. Acoustic field

In an acoustic-based micromixer, the pressure fluctuations induced by the propagation of the acoustic wave disturb the laminar-flow fluids to facilitate mixing (Table 2) [72]. The sharp-edged structure is one of the most common structures for this type of micromixer. This is because the strong acoustic vortex intensity at the sharp corner allows the micromixer to operate at a relatively low power input, which avoids any local heating generated by the piezoelectric actuator and makes it suitable for fluids that are sensitive to temperature changes [73].

To identify the geometric sharp-edged configuration with the best mixing performance, Zhang et al. conducted a comparative study on the design schemes of three sharp-edged structures, S1, S2, and S3, in the mixing channel, as shown in Fig. 9 [74]. According to the simulation and experimental results, the S2 structure showed the best mixing

performance, especially for fluids with a low Reynolds number ( $Re$ ), due to the more proper distance between the adjacent sharp edges. In addition, the smaller the angle of sharp edge, the better the mixing performance. Given the actual fabrication technology, however, an angle of  $30^\circ$  can minimize the chance of splitting during the fabrication process. Meanwhile, although the mixing degree of acoustic-based methods decreases as the flow rate increases, these methods can be utilized to enhance the mixing degree in passive structures. Therefore, a combination of two methods can greatly increase the range of effective flow rates [75]. As shown in Fig. 10, acoustic streaming was generated by oscillating the sharp-edged structure, and the Tesla structure achieved hydrodynamic mixing. In the proposed micromixer which combined the acoustic field with a passive structure, the effective flow rates ranged from 20 to  $2000\text{ }\mu\text{L}/\text{min}$ , with the mixing index kept above 0.9. The practical applicability of this method was demonstrated by synthesizing PLGA-PEG nanoparticles with sizes differing by two orders of magnitude at flow rates of 20, 400, and  $2000\text{ }\mu\text{L}/\text{min}$ . The results showed that the size distribution decreased from  $93.76\text{ nm}$  to  $64.51\text{ nm}$  as the flow rate increased. The acoustic streaming phenomenon can be strengthened by coupling some bubbles in the sharp edges in the channels because the gas in the bubbles can cause the interface of the bubbles to be expanded or contracted by five percent of its initial size [76]. However, the most important thing is to design a combination scheme to maximize the fluid mixing efficiency [77]. As shown in Fig. 11, the bubbles and sharp edges were combined in close proximity. This made it possible to perform volume pulsation on the bubbles as a secondary acoustic transmitter to increase the vibration of sharp edges. Three factors were selected to optimize the mixing performance. The first one was the frequency of the piezoelectric transducer, i.e., the resonant frequency of the bubbles and the piezoelectric transducer corresponded to the maximum driving pressure. The second one was the input voltage, and an input voltage of  $14\text{ V}_{\text{pp}}$  corresponded to the optimal mixing performance. The third one was flow rate, which just as in other methods, was inversely proportional to the mixing performance. Finally, this structure was utilized to synthesize PLGE-PEG nanoparticles and liposomes as hollow nanoshells for application in pharmaceutical and biomedical fields. The most remarkable feature of this structure is that it can guarantee homogeneity of fluids at very high flow rates. Specifically, it can complete mixing within  $0.8\text{ ms}$  at a flow rate of  $116\text{ }\mu\text{L}/\text{min}$ . Therefore, the nucleation of amphiphilic precursors can be maintained in a homogeneous environment without nanoparticle aggregation.

Using microfluidic chips for microfluidic mixing has two significant advantages, shorter time and more homogeneous mixing. For example, a novel acoustically enhanced micromixer was proposed to synthesize highly homogeneous budesonide nanoparticles [78]. In this micromixer, a vibrating membrane was embedded in the microchannel to interact with the surrounding fluid media. Then, the membrane was excited at its resonant frequency by the piezoelectric transducer, which induced an

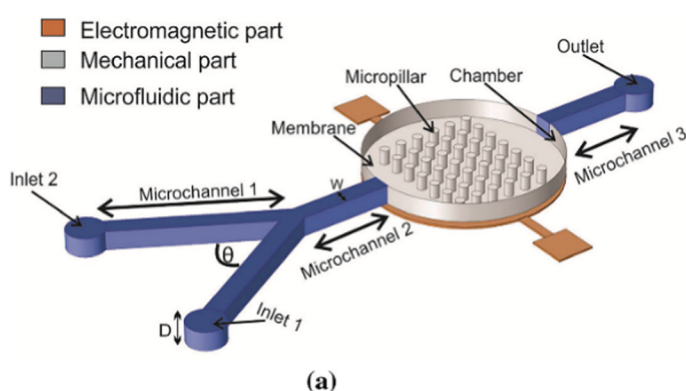


**Fig. 7.** Schematic of a representative microfluidic mixer structure. (a) An active microfluidic mixer. (b) The membrane [69].

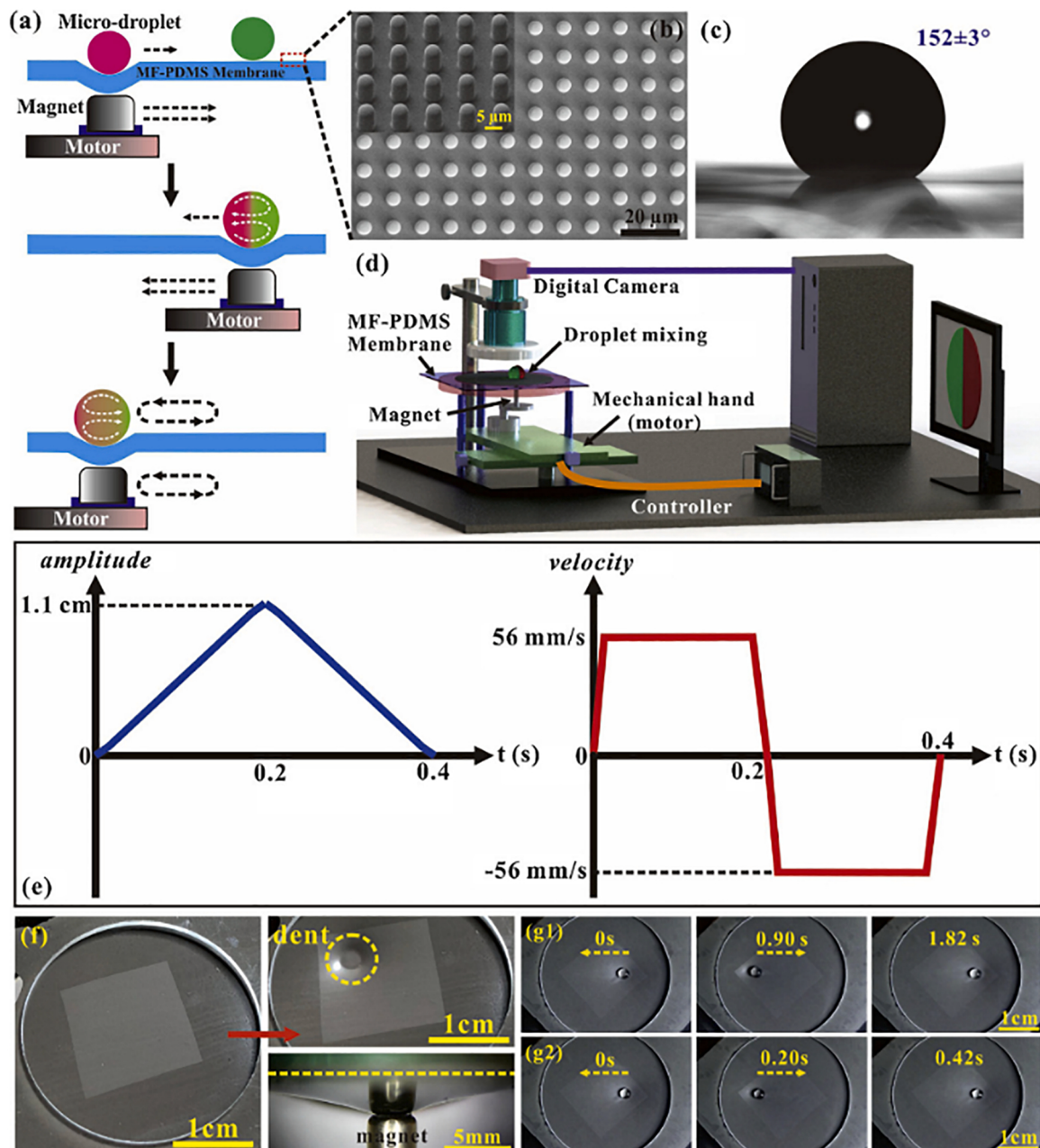


**Fig. 8.** (a) Schematic of the working mechanism of the proposed 'open-surface' microfluidic platform for rapid and efficient microdroplet mixing; (b) SEM image of the micropillar array integrated on the magnetically functionalized PMDS membrane; (c) Static contact angle of the microdroplet on the as-prepared super-hydrophobic magnetic PDMS membrane; (d) Schematic of the experimental setup for controlled mixing actuation and real-time monitoring of the mixing efficiency; (e) Wave profiles of the amplitude (left) and velocity (right) in the back-and-forth motion under the frequency of 2.5 cycles/s; (f) Optical images of the MF-PDMS membrane attached to the glass holder with and without the magnet placed underneath as the dent appears; Serial images of microdroplet position manipulations by external actuation under driving frequencies of (g1) 0.5 cycle/s, and (g2) 2.5 cycles/s [71].

acoustic flow field and strong vortices to increase the mixing performance and efficiency. Using dynamic light scattering (DLS) to measure the particle size with and without the action of the acoustic field, it was verified that this structure has great advantages in improving particle uniformity. In addition, the nanoparticles synthesized by this method were up to 40 times smaller in size than those by previous methods. This feature empowered drugs with much improved solubility, thus increasing the bioavailability of drugs. A novel high-throughput acoustically driven micromixer was developed and its maximum effective flow rate reached 8 mL/min, 50 times higher than that obtained in previous methods [79]. As shown in Fig. 12, the device consisted of two layers of PDMS, a lower layer which guided fluids to the mixing channel

and an upper layer which was connected the outlet channel. There was a micromechanical oscillator between the two layers. When the MHz frequency power was input to the piezoelectric transducer, a strong acoustic streaming field was produced in the sharp edge of the oscillating plate. The structure of the oscillator was designed to be a polygonal sharp consisting of some point stars. By comparing the optimum conditions, including the driving frequency and flow rate, it was determined that eight-point stars delivered the best mixing performance. Furthermore, to verify the practical applicability of this structure, some budesonide nanodrugs and DNA nanoparticles were synthesized for a comparison with traditional methods. The diameters of these nanoparticles were measured by DLS. The results showed that the

**Table 2**  
Mixing performance of acoustic-based micromixer.

Categories	Mixing technique	Mixing index	Reference
Sharp-edged structure	30° sharp edges	≈ 99%	[74]
	Tesla structure	≈ 99%	[75]
	Combine bubbles and sharp edges	90%	[77]
	Polygonal sharp consisting of some point stars	94%	[79]
Other designs	Dome-shaped chamber	90%	[81]
	Micromixer with a membrane-type valve	90%	[84]
	Multi-node standing waves	96%	[85]

diameter of the budesonide nanodrugs was  $80 \pm 22$  nm and that of the DNA nanoparticles was  $63.7 \pm 24.7$  nm. Compared to other methods, this method delivered a higher mixing throughput and the synthesized

nanoparticles were smaller in size and exhibited a narrower distribution of size. To make full use of the acoustic energy of surface acoustic waves (SAWs) to improve the mixing efficiency, Ahmed et al. proposed an interdigitated transducer (IDT)-based acoustic mixing scheme [80]. The structure consisted of two inlets and two outlets on the straight micro-channel, and the IDT was placed right underneath the first outlet, which produced high-frequency surface acoustic waves. The sample flow was vertically stirred by the sheath flow via a SAW-induced acoustic streaming flow to enhance the mixing performance of two samples. The complete mixing of this structure required a flow rate of  $50 \mu\text{L}/\text{min}$  and an input voltage of  $12 \text{ V}_{\text{pp}}$ . Furthermore, the mixing efficiency can be kept above 90% as the flow rate increased to  $200 \mu\text{L}/\text{min}$  and the voltage remained unchanged.

Some other designs have been proposed to expand the application scope of the acoustic field. For example, Lim's research group first proposed a dome-shaped chamber-based SAW micro-mixer structure

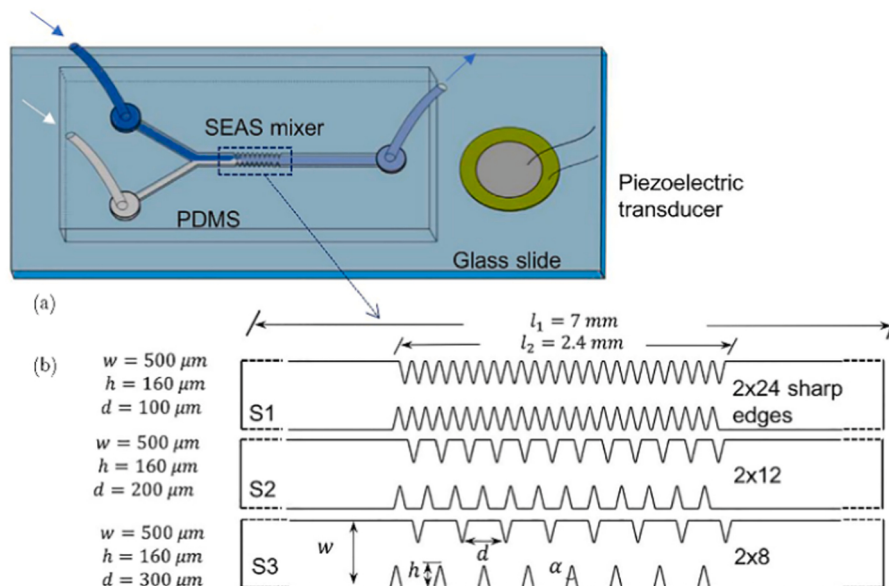


**Fig. 9.** (a) Experimental setup with the microchannel and the transducer glued on the upper coverslip. (b) Three different geometric structures tested, with  $n_s = 24$ , 12, and 8 sharp edges on each side and varying distance  $d$  between the tip of two adjacent edges [74].

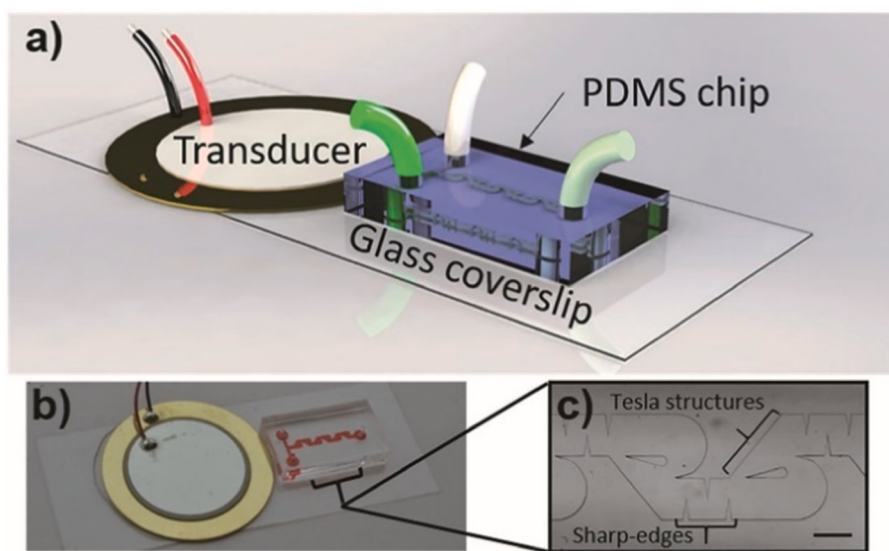


**Fig. 10.** (a) Schematic of the acoustofluidic mixing device. (b) A photo of the acoustofluidic mixing device with a close-up (c) of the microfluidic channel design. Sharp edged structures (vertical) and recirculation zones (rounded sections) can be seen in the channel [75].

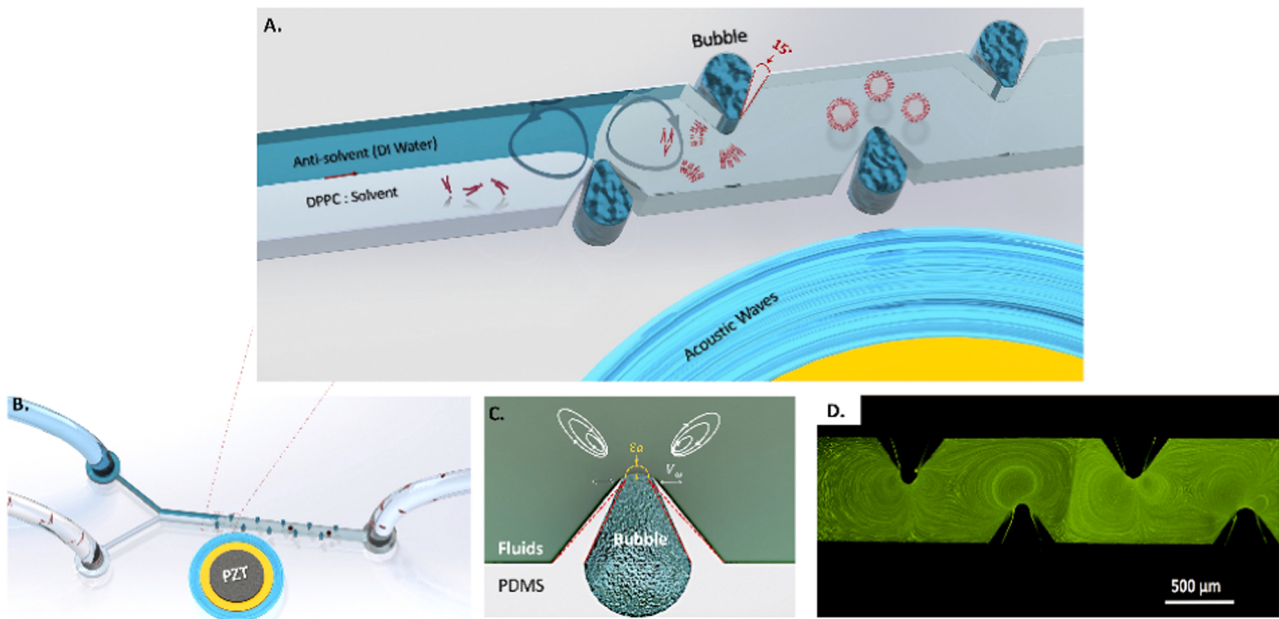


**Fig. 11.** (a) Conceptual illustration of the acoustic streaming and the resultant mixing used for self-assembly of nanoparticles. (b) Rendered picture of the acoustic platform. The piezoelectric transducer was embedded next to the PDMS part, emitting acoustic pressure waves. (c) Schematic of the combination unit. Slanted sharp edges allowed the bubble to be trapped. (d) The behavior of fluorescent polystyrene particles (2  $\mu\text{m}$  in diameter) in the presence of the acoustic field. The closed-circular pathline of microparticles covered the entire width of the channel [77].

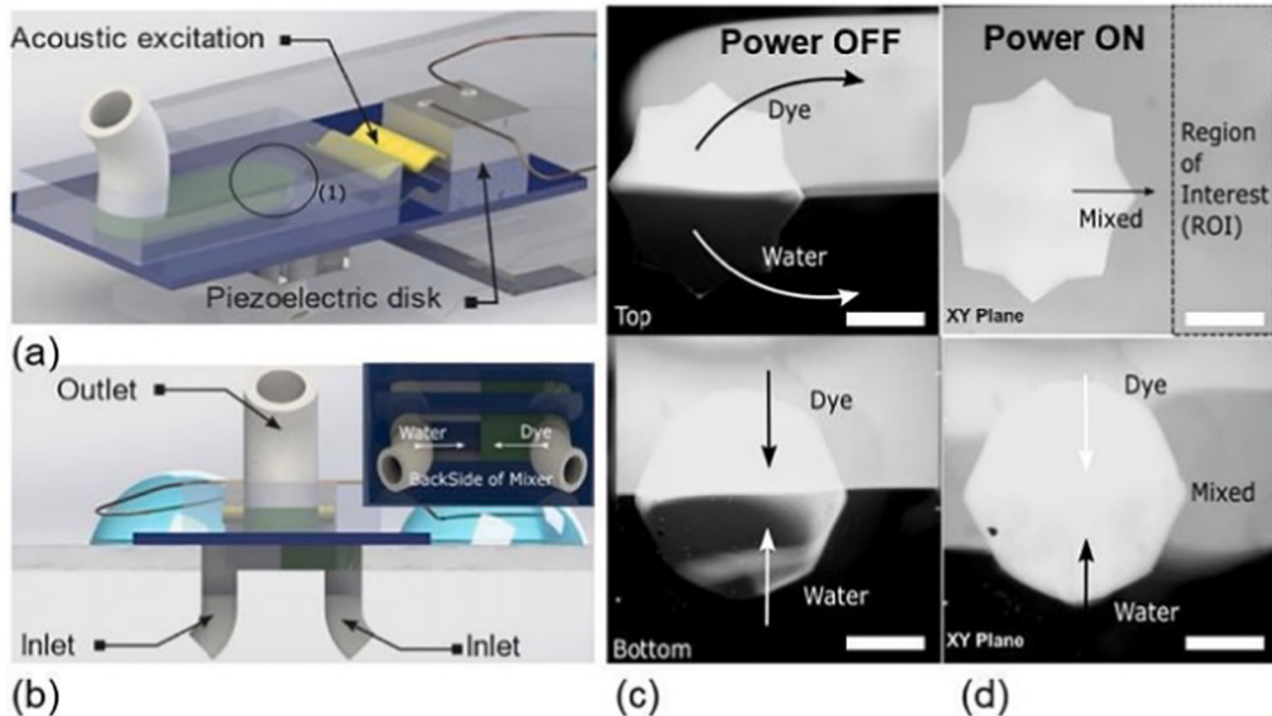


**Fig. 12.** (a) Schematic of device. (b) Side view showing the inlets and outlet. (c) Experimental snapshots showing the fluid flow (2 mL/min) before activation and (d) after a 1 MHz AC signal was applied to the piezoelectric element resulting in incomplete mixing. Mixing started at the bottom surface where the reactants were fed into the oscillating structure, and ended at the top surface; the dashed line black box indicates the region where the relative mixing index was estimated [79]. (Scale bar is 500  $\mu\text{m}$ .)

[81]. To solve the limitation that the droplets were unstable during SAW propagation, the contact angle of the dome-shaped chamber was selected to be about 68° because the Rayleigh angle of 22° can maximize the propagation of SAWs, as shown in Fig. 13. Another advantage of this device was its ease of fabrication, which only required a single adhesive

tape and a UV-curable material. The concentrated acoustic energy generated by the focusing transducer was applied to the dome-shaped chamber, and the mixing efficiency was enhanced with the increase of voltage and the decrease of flow rate. According experimental results, the mixing index was higher than 90% at a voltage of 20 V and a flow

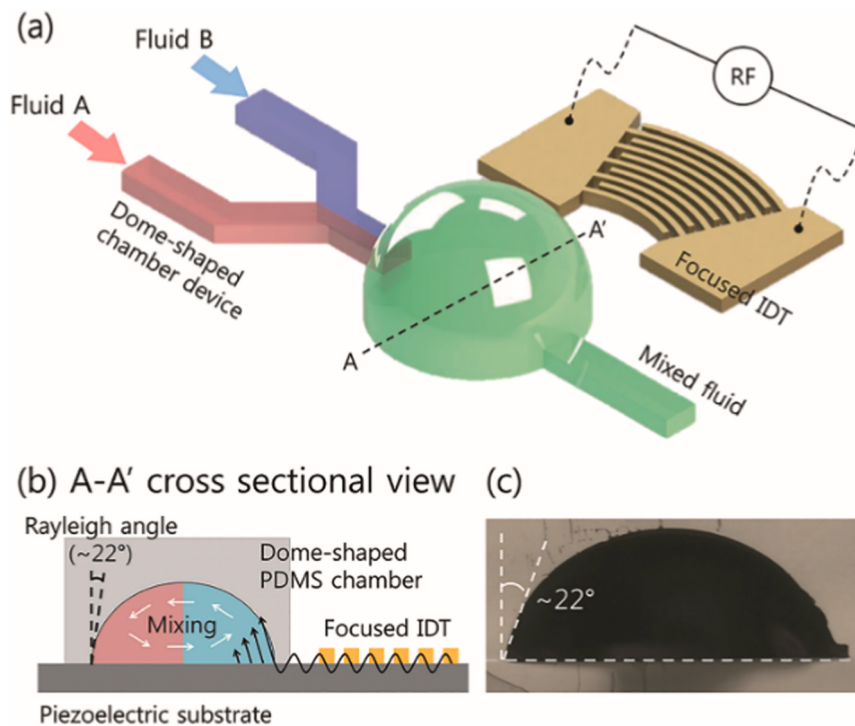


**Fig. 13.** (a) Schematic of the dome-shaped chamber for micromixing using SAWs. Fluids A and B were injected into the inlets. By applying an RF signal to focused interdigital transducers (IDT) (F-IDTs), the concentrated acoustic energy was generated, and two fluids were mixed in the dome-shaped chamber. (b) Cross-sectional image of the dome-shaped chamber on line A-A' depicted in (a). (c) Cross-sectional image of the dome-shaped chamber device fabricated for acoustic mixing [81].

rate of  $300 \mu\text{L}/\text{m}$  of. Therefore, the successful design in open droplet systems made this structure applicable in many fields, such as droplet jetting [82] and droplet atomization [83]. The volumetric restrictions of the reaction chamber usually influence the efficiency when the exact reaction is not yet defined. Therefore, Zhang et al. developed an acoustic micromixer with a membrane-type monolayer valve to flexibly control the volume of the reaction chamber [84]. This valve was pressurized and closed at the beginning, and the volume of the fluid to deliver into the mixing chamber was controlled by adjusting the pressure on the valve. Meanwhile, the high mixing efficiency induced by SAW ensured that the fluid flowing in the chamber through the valve could be mixed fully in a short time. After testing  $44.3 \text{ nL}$  of samples, it was determined that the best mixing performance was achieved when the frequency of the applied power was  $70 \text{ MHz}$ , and the time it took to mix these samples was reduced to  $1.5 \text{ s}$ . It has been found that non-homogeneous fluids under the action of acoustic standing waves can lead to the re-localization of fluids to some stable configuration under the action of non-dissipative acoustic force density. Potluri et al. used the fluid migration principle to drive and mix fluids with bulk acoustic waves [85]. The principle of mixing was to utilize the variable acoustic force density by means of alternating multi-node standing waves, which would produce more parallel stratification and stronger chaotic advection and facilitate rapid mixing. The influence of the initial configuration parallel and perpendicular to the fluid interface on the mixing was demonstrated by an experiment on the solution concentration distribution. The results showed that the mixing performance when the standing wave acoustic field was parallel to the interface was better than when it was perpendicular to the interface. It should be noted that this method can only be used for fluids with different densities or acoustic velocities. The results showed that fast and efficient mixing could be achieved by applying multi-node standing waves in a direction parallel to the initial fluid flow interface, regardless of the initial flow state.

### 2.3. Electric field

In active micromixing methods, the electric-based method offers unique advantages such as easy fabrication of mounted electrodes, the absence of any moving parts, and the use of small voltages, making it an attractive mixing mechanism for many biochemical analysis applications (Table 3) [86].

In the microchannel, when the solid wall comes in contact with the electrolyte solution, the surface of the solid wall is hydrolyzed and charged, attracting foreign heterogeneous ions close to the wall surface. According to this phenomenon, an induced-charge electroosmotic micromixer was proposed, which was designed with a simple structure and easy to fabricate [87]. As shown in Fig. 14, six rectangular floating electrodes were asymmetrically arranged in the microchannel. The driving electrodes extended the main channel, which made it applicable to the external electric field. Furthermore, the internal electrodes led to the formation of a double electric layer, and the surrounding electroosmotic flow generated vortices to facilitate fluid mixing. Then, the effects of fluid viscosity, frequency, flow rate, AC signal type, voltage, and other factors on the mixing efficiency were investigated. The results showed that the mixing efficiency reached 94.7% at a flow rate of

**Table 3**  
Mixing performance of electric-based micromixer.

Categories	Mixing technique	Mixing index	Reference
Electroosmotic micromixer	Six asymmetrically arranged electrodes in channel	94.7%	[87]
	Three electrodes were placed at the inlet and outlet	95%	[88]
	Three-finger sinusoidal electrode in channel	90%	[89]
	Corrugated channel	97.53%	[90]
Light-driven AC electroosmotic micromixer	Specific optical pattern	97.65%	[96]

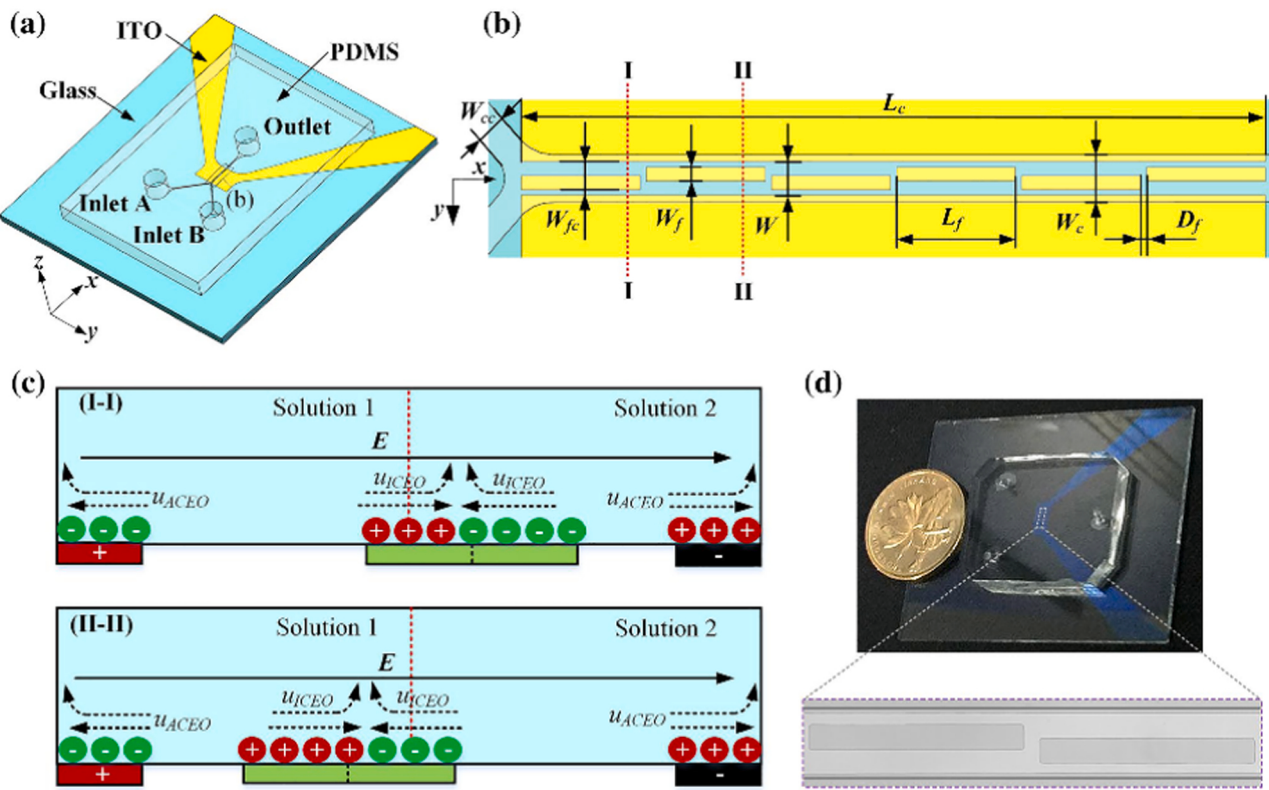


**Fig. 14.** (a) Schematic of the electro-fluidic device for on-chip fluids mixing. (b) The top view of the main channel showing six floating electrodes asymmetrically arranged. (c) The principle of fluid flow on the cross-sections of the channel (cross-sections I-I and II-II, are defined in b). (d) A photo of the micromixer [87].

1500  $\mu\text{m}/\text{s}$ , and the input power was a sinusoidal wave with a frequency of 400 Hz and a peak voltage of 14 V.

A novel induced-charge electrokinetic micromixer was proposed with an aim to shorten the mixing length and simplify the fabrication process [88]. Three electrodes were placed at the inlet and outlet of the micromixer to generate an external electric field and an electroosmotic flow in the side microchannel. Due to the vortices generated around the conductive surface of the mixing chamber, most of the mixing process was completed in this chamber. Specifically, a diamond-shaped mixing chamber with one conductive surface and conductive edges had the highest mixing efficiency, which was about 95%. The entire experiment was conducted in a simple chip structure with high efficiency and a short mixing length.

A field-effect mixer with a phase-controlled three-finger sinusoidal electrode was proposed based on the concept of AC permeation [89]. Three sinusoidal s-shaped electrodes were placed parallel to the main channel on a Y-shaped microchannel, with the electrodes on either side of the gate, which was denoted by the middle electrode, interchangeably designated as the source and drain electrodes. An asymmetric lateral flow was generated under a low-pressure drive to allow mixing to occur. Optimal mixing occurred when the potential difference between the gate and the source was greater than that between the source and the drain. Comparative studies revealed that the optimal frequency for mixing was around 40 kHz, and the mixing performance would increase with the increase of voltage. By adjusting the phase hysteresis between drive voltages at constant amplitudes, the distribution and intensity of the electric field can be changed, resulting in different AC permeation slip rates and mixing performances. The experimental results showed that the mixing efficiency can reach more than 90% at a flow rate of 4  $\mu\text{L}/\text{min}$ . The mixing efficiency of the device could also be improved by adjusting the phase shift between electrodes, which would help to produce nanoparticles with increased monodispersity and concentration.

To improve the mixing efficiency, Najjaran et al. developed a novel

induced-charge electrokinetic micromixer by combining two mixing methods, corrugated wall and conductive plate [90]. As shown in Fig. 15, four different shapes of corrugated wall micromixers were designed. The presence of corrugated walls caused an abrupt change in the fluid flow path, which interrupted the flow and allowed mixing to occur. Electrodes were placed at both ends of the micromixer to generate an electric field that applied a potential difference, and the conductive plates within the mixing channel generated an induced electrical penetration that created two opposing vortex flows. Several factors needed to be considered, including the number of conductive surfaces of the mixing chamber, the size of the mixing chamber, electric field strength, the placement of the conductive plates, and the length of the conductive plates. For example, the conductive plate was placed under the corrugated microchannel near the inlet section and the electric field intensity was set to 40 V, the final mixing efficiency can be improved several times. After optimizing all the factors, the maximum mixing efficiency reached 97.53%.

Although a high voltage can increase the vortex around the electrodes, it has a non-negligible impact on the samples and electrodes as it causes overheating. Wu et al. proposed a novel low voltage electroosmotic micromixer with a fractal structure to achieve a high mixing index [91]. The fractal structure had three pairs of electrodes, which meant a stronger electric field force and more pronounced chaotic convection, contributed to the high mixing efficiency. After optimizing three parameters, i.e., the position, length, and spacing of the electrodes, the mixing index reached a maximum of 95.2% in one second. A similar structure design scheme was utilized by Xiong et al. to investigate the mixing performance of a fractal structure with a DC voltage [92]. The simulation results showed that the mixing efficiency could reach 98% when the DC voltage was 10 V and the electrode spacing was 0.15 mm.

Usefian et al. proposed a micromixer in which an electrode array was located on the surface of the microchamber. First, a rotating cylindrical obstacle was placed in the interior part of the chamber to create a strong

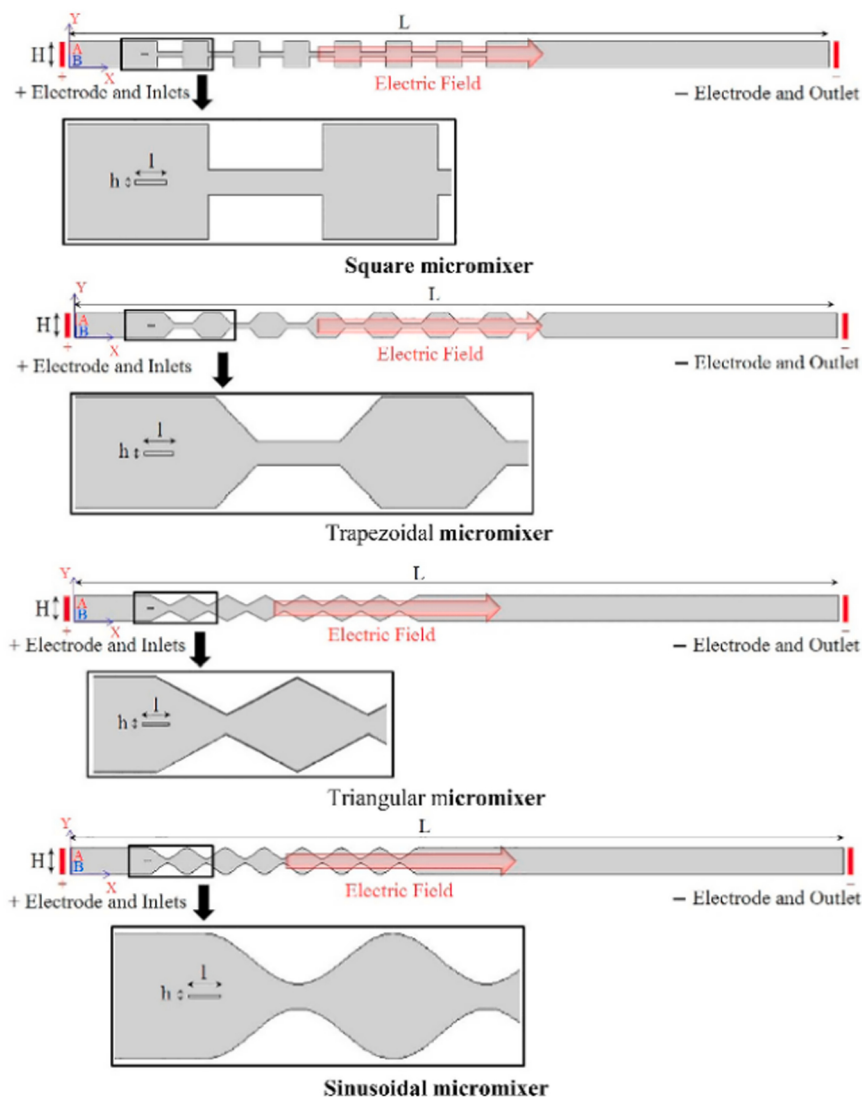
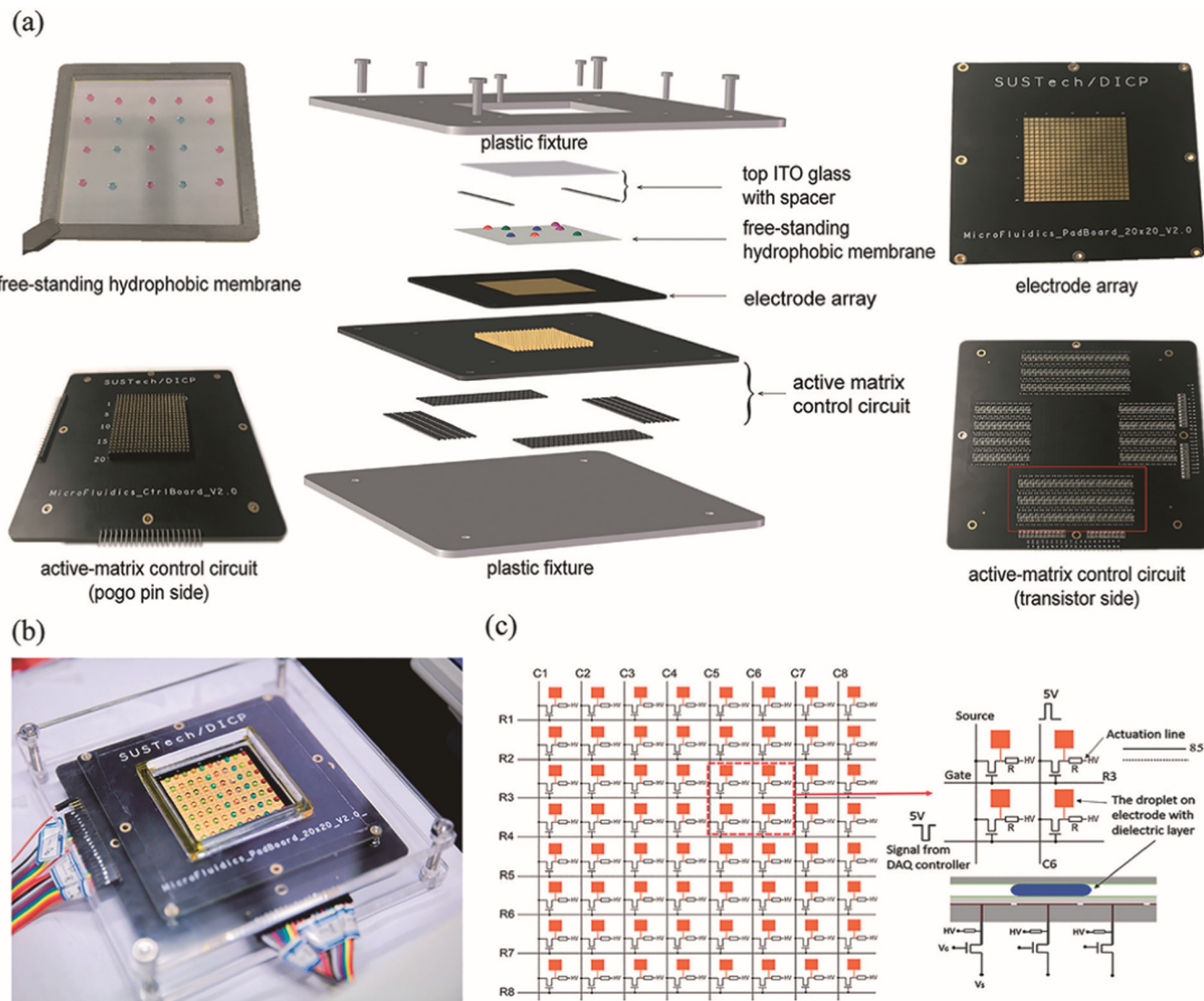


Fig. 15. Schematic of a micromixer in a square, trapezoidal, triangular, and sinusoidal shape [90].

circulation area. Then, the radius of the cylindrical obstacle and physical properties of electric and fluid fields were optimized by simulation to determine the optimal mixing index [93]. The results showed that the mixing performance increased dramatically with the increase of AC frequency, voltage value, and angular velocity of the obstacle, and the increase of fluid velocity was beneficial to the final mixing degree. An optimal set of parameters can bring the mixing index up to 97.67%. In particular, the device exhibited a higher mixing efficiency for non-Newtonian fluids than for Newtonian fluids. Xing et al. developed a highly reliable, low-cost, and scalable digital microfluidic platform [94]. As shown in Fig. 16, the platform consisted of four parts, including an active array control circuit board, an electrode array board, a hydrophobic polymer membrane, and an indium tin oxide glass (ITO) plate. The researchers designed a reliable method for driving droplets with different ion contents. The device could synthesize pentapeptides in 30 min, compared to 8 h by other commercial devices. The device could drive droplets at a low voltage and operate for a long time without electrical breakdown. A specially designed replaceable hydrophobic polyethylene terephthalate/Teflon bilayer membrane was used to avoid contamination between experiments. By fully using the potential of this digital microfluidic platform, this device showed good potential for automation of high-throughput analytical and synthetic tasks in chemical engineering, bioengineering, and biomedical engineering.

Zhou et al. developed a self-powered droplet manipulation system (SDMS) that allowed for precise manipulation of liquid droplets mixing [95]. As shown in Fig. 17, a triboelectric nanogenerator (TENG) was used to provide power and connected with diode to convert power to pulsed DC voltage. Furthermore, the electric brush distributed different charges to the electrodes, which caused a high electrostatic field to be generated between the electrodes. Therefore, different liquid droplets could be controlled under the action of Coulomb's force by tuning the brush. The droplets could be mixed by elongating, retracting and rotating them in different directions. In particular, the device could reduce the mixing time by 6.3 times compared to passive methods, while increasing the velocity of droplets to 52 mm/s and their volume to 400  $\mu$ L. The device can perform various operations on liquids without an external power source, which gives it an edge in chemical transfer, biochemical analysis, inkjet printing, and more.

To reduce the fabrication difficulty and improve the functional flexibility of microchips, the light-driven AC electroosmotic technology for microfluidic mixing was applied to solve the coupled system of flow, electric, and concentration fields using a finite element method [96]. As shown in Fig. 18, two ITO glasses were arranged in the upper and lower layers of the mixing channel, and the lower layer of was set with a photoconductive layer. When a specific voltage signal was applied to two ITO glass layers and a specific optical pattern was projected onto the



**Fig. 16.** (a) The components and an exploded view of the active-matrix digital microfluidic system; (b) a photo of the assembled digital microfluidic platform; (c) Schematics of the active-matrix circuitry and the biasing scheme for droplet actuation [94].

surface of the photoconductive layer, different partial pressures were generated in the bright and dark regions, and a non-uniform electric field was thus generated in the microchannel. Therefore, the resulting electrically permeable rotating vortices could enhance the mixing performance by perturbing and folding fluids. Factors affecting the mixing efficiency included applied potential, electric field frequency, and average inlet velocity. Experimental results showed that the mixing index was the highest when the potential increased to 5 V and the frequency was kept below 10 Hz. This method provides a new approach to efficiently mixing liquids in modern microfluidic analysis systems with versatile functions, a simplified chip structure and reduced chip fabrication costs.

#### 2.4. Thermal field

The electrothermal phenomenon occurring in conductive fluids can be utilized to promote the flow and mixing of fluids in a micromixer chip. The temperature gradient caused by this phenomenon gives rise to a gradient change in the physics properties of the electrolyte fluids (e.g., conductivity, dielectric constant, density, and viscosity), which in turn results in a bulk force that can drive the flow and mixing of fluids [97, 98].

Ramiar et al. conducted a simulation study to look for the chip design best suited for making good use of this phenomenon [99]. In the three geometries, the geometry with a trapezoidal chamber and a circular cavity showed better efficiency, and the width of the channel was proportional to the intensity of vortices and inversely proportional to flow velocity. In addition, the higher electrical conductivity of the fluids induced lower mixing efficiency and higher temperature in the fluids. Thus, this method has strict requirements regarding the temperature adaptability of the fluids. An AC heating method was proposed for mixing highly conductive fluids with high efficiency [100]. AC heating was uniquely capable of producing the nonuniform Joule heat in fluids, which would cause temperature gradients and further induce changes in the electrical conductivity of fluids. As shown in Fig. 19, the AC electrodes were installed at the bottom of the micromixer channel. In particular, a thin-film heater was also installed for more flexible control of channel temperature. In addition, A passive structure was adopted to increase the mixing degree. After the parameters of voltage, conductivity, electrode width, and thin-film heater size were through simulation, the mixing efficiency of the thin-film heater was increased to 90%. More importantly, the temperature of fluids can be thus optimized, not only to meet the extremely high requirement for mixing degree, but also to help mix cell culture fluids in the biological field. In their subsequent

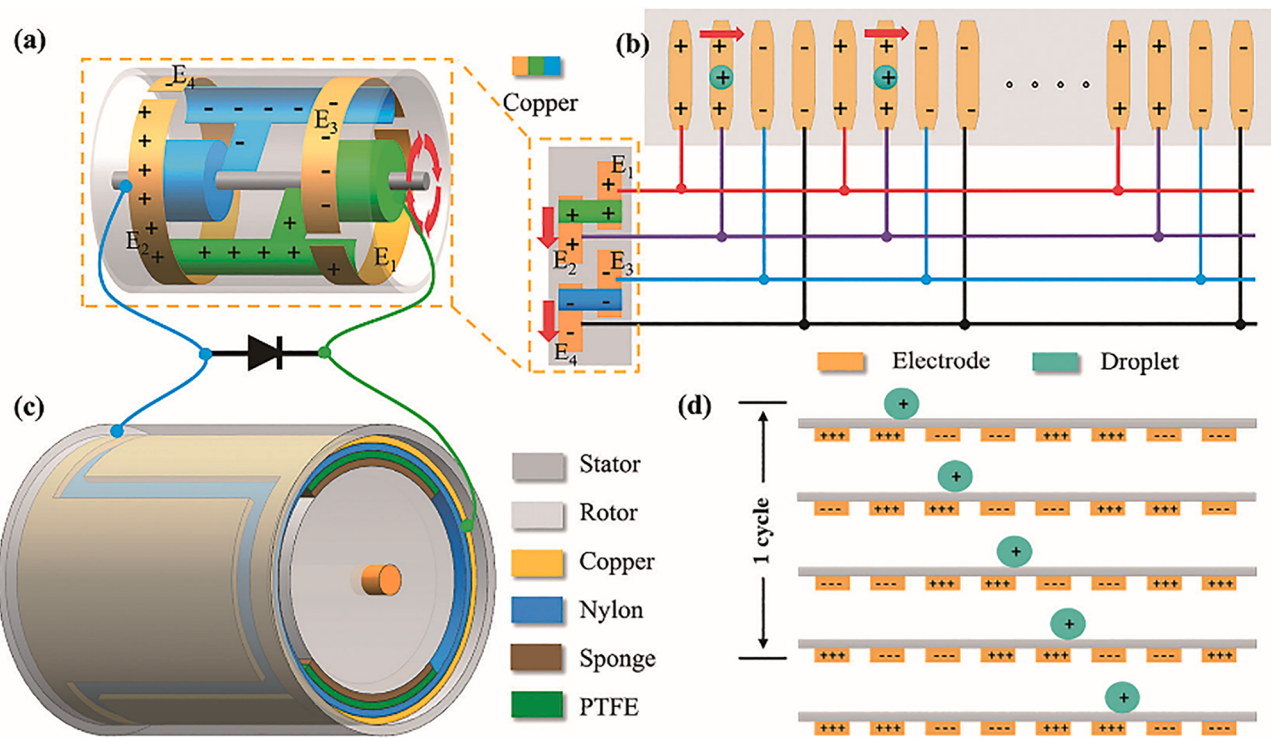


**Fig. 17.** Schematic of a self-powered droplet manipulation system for transport of droplets. (a) Electric brush. (b) Schematic of the droplet-based long-distance transport system. (c) Structural design of the rotating freestanding TENG. (d) The moving track of the droplets under the action of sequential voltages applied to the electrodes [95].

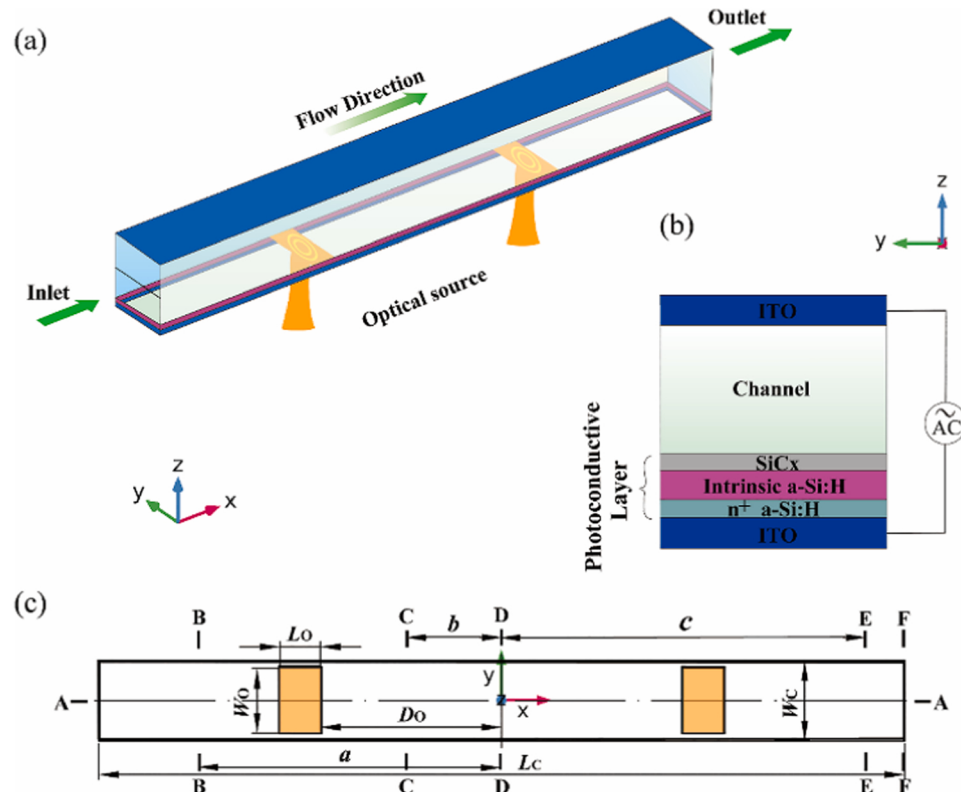


**Fig. 18.** Schematic of the microfluidic mixer based on the light-actuated oscillating electroosmosis in a low-frequency sinusoidal AC electric field. (a) The 3D structure of the microfluidic mixer, with green arrows indicating the flow direction. (b) Cross-sectional (yz) view of the microfluidics mixer and photoconductive layer. (c) The top view of the photoconductive surface. The orange areas indicate the symmetric light spots projected onto the photoconductive layer. A-A represents the longitudinal section (xz section) at the center of the microchannel. B-B, C-C, D-D, E-E and F-F represent the yz sections at a distance of  $-75 \mu\text{m}$ ,  $-25 \mu\text{m}$ ,  $0 \mu\text{m}$ ,  $+90 \mu\text{m}$  and  $+100 \mu\text{m}$  (outlet position) from the center of the microchannel, respectively. The origin of the Cartesian coordinate system is located at the center of the photoconductive surface on the bottom [96].

studies, the researchers used a genetic algorithm to select four optimal design parameters from 30 sets of design points, including the width-to-length ratio of the AC electrode, the inlet velocity, the voltage

amplitude, and the heat of the film heating sheet [101]. After these four parameters were optimized, tri-objective optimization was achieved, a higher mixing index, lower temperature rises and lower mixing energy

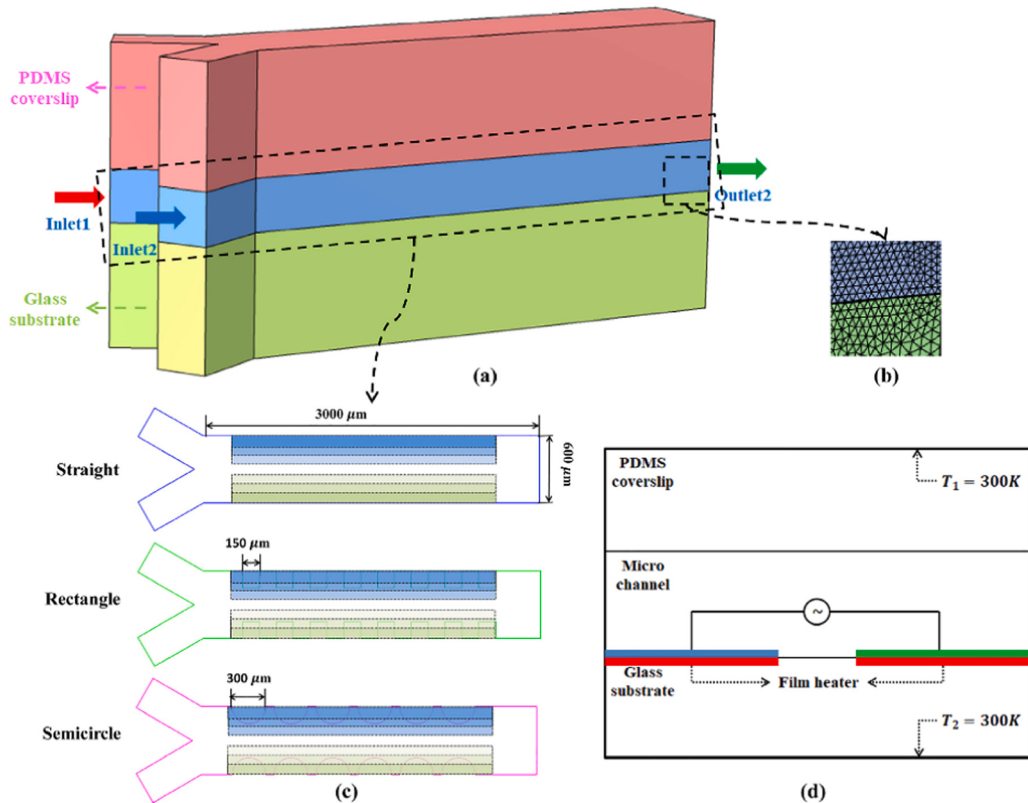


**Fig. 19.** (a) 3D modeling of the micromixer, (b) mesh division, (c) three different channel structures, electrode positions and size ranges, and (d) the position of the electrode and the film heater and the setting of the temperature boundary based on the AC electric heating micromixer model [100].

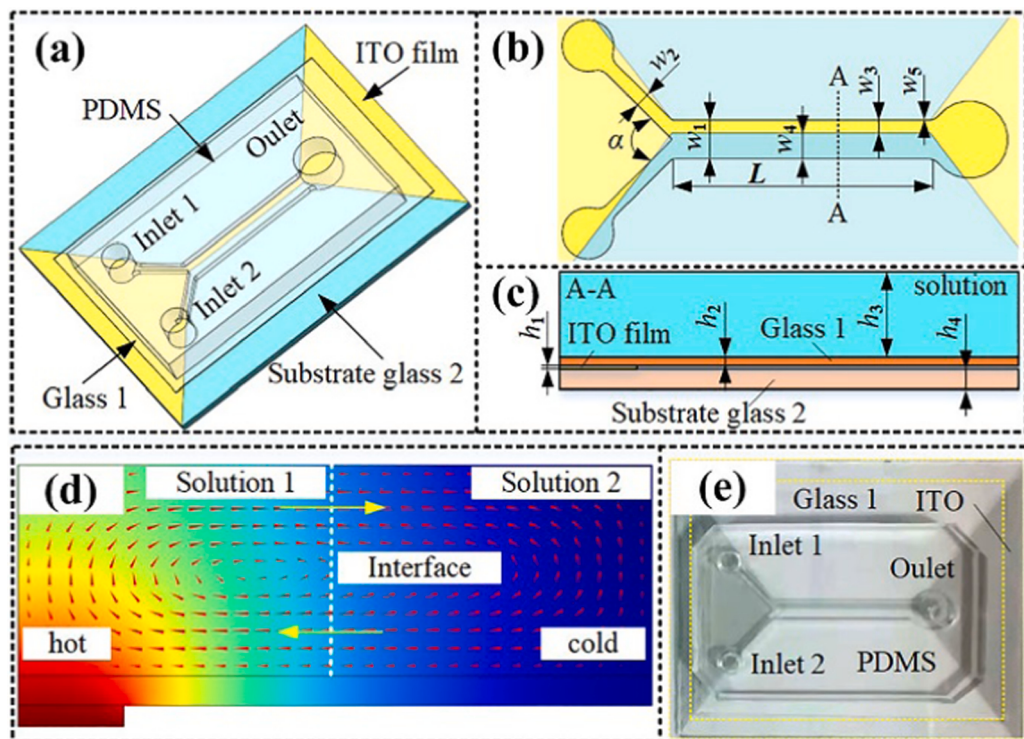


**Fig. 20.** (a) 3D schematic of the micromixing device. (b) Top view of the micromixer. (c) Side view of the main channel. (d) Mixing mechanism: The vortices induced by buoyancy flow can disturb the fluidic interface and improve the convective mass transfer of two fluids. The enhanced liquid temperature also enables an improved diffusive mass transfer process as the diffusion coefficient  $D$  increases with the temperature. (e) Photo of the micromixing device [102].

costs. To improve the efficiency and economy of thermal-based approaches, Zhang et al. proposed a novel method for continued microfluidic mixing based on a DC-induced micromixer [102]. As shown in Fig. 20, an ITO microheater was placed at the bottom of the micro-channel asymmetrically and powered by DC, and under the action of the asymmetrical thermal field, thermal buoyancy convection was formed to promote fluid mixing. The most controllable DC voltage is positively related with the mixing efficiency, and this feature makes it easier to synthesize different nano-sized  $\text{Cu}_2\text{O}$  particles. Considering that the mixing index can reach 97.3% at a voltage of 8 V, the voltage range was set to be from 5 V to 8 V, and the mixing index increased from 13.5% to 97.3%. Therefore, the particle size decreased from 0.967  $\mu\text{m}$  to 0.680  $\mu\text{m}$  over this voltage range, while the standard deviation of particle size decreased due to the more uniform mixing performance.

The combination of tri-objective optimization of an AC electro-thermal micromixer with the fractal principle was first proposed by Lv et al. [101]. The width to length ratio ( $a/b$ ), inlet velocity ( $U$ ), voltage amplitude ( $V$ ), and heat of the thin-film heating sheet ( $Q$ ) of the AC electrode based on the Cantor fractal were used as design variables. The mixing index, temperature rise, and mixing energy cost were used as the objective functions. By weighing the three objectives, the micromixer with a high mixing index, a low temperature rise, and low mixing energy consumption was selected as the main objective from the obtained Pareto optimal solution set. The Pareto genetic algorithm was used to optimize the agent model and obtain the Pareto optimal surface, and the basic principle is shown in Fig. 21. The results showed that the optimized micro-mixer delivered a 19.81% higher mixing index and a 73.16% lower mixing energy cost compared to the reference design. This multi-objective optimization approach is expected to make a bigger contribution to researches on cell culture fluid mixing and biochemical reactions.

## 2.5. Passive methods

In contrast to active methods, passive methods do not require extra energy to improve the mixing efficiency and do not involve any complex channel design [103]. Therefore, passive methods are more widely applicable. Basically, passive methods utilize some special geometric structures of microchannels to produce irregular vortices and chaotic advection [104]. In addition, some microchannel shapes were designed to improve the area and length of contact between two fluids to improve the mixing efficiency [28]. All of these designs focused on how to improve the efficiency of molecular diffusion [105]. Passive methods also offer a very creative approach to the design of microchannel structures. In addition to these two representative designs, many other designs have been developed, such as multi-layer structures [40] and channels with grooves [106]. In this paper, we classify those structures into three representative structures, including specially designed channel structures, obstacle-based structures, and some other distinctive structures (Table 4).

A specially designed channel structure induces fluid disturbance by changing the cross-sectional area of the channel. The most representative design is a curved microchannel structure, which stretches fluids in the outer circle of the channel and folds fluids in the inner circle. For this structure, Liu's research group proposed a structure optimization scheme to achieve higher mixing efficiency [29]. In a serpentine micromixer, the pressure drop ( $\Delta P$ ) between the inlet and the outlet is a factor that determines the energy to consume and the stability of the mixing performance. Therefore, the researchers studied how structural parameters of the microchannel affected the value of  $\Delta P$ . First, they proposed a curved channel structure with elliptic curves, and the focal length was taken as the primary parameter to optimize. After comparing simulation and experimental results, they found the foci of the elliptic channel on the X-axis exhibited better mixing performance, as shown in Fig. 22(b). With this feature, this structure can maintain smooth drop of

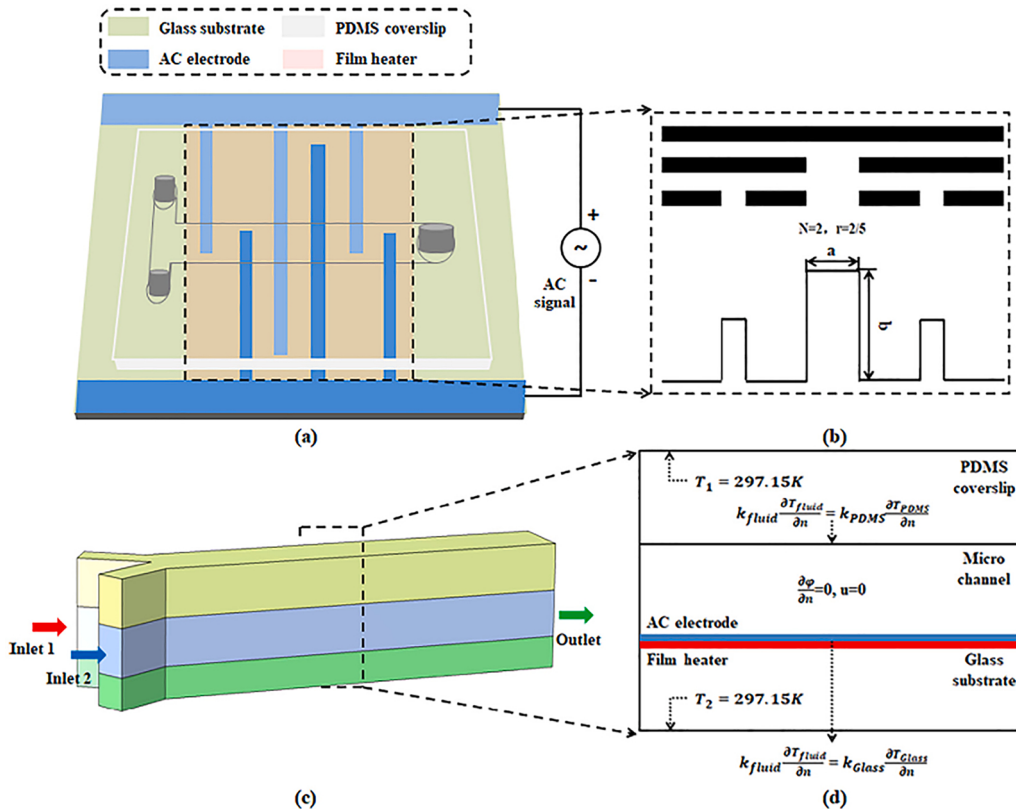
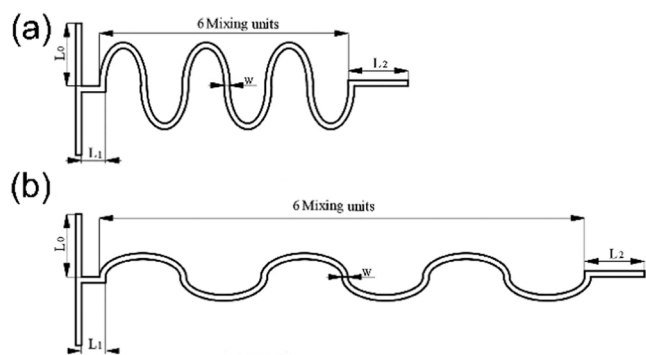


Fig. 21. 3D modeling of the micromixer. (a) Schematic of the micromixer based on AC electric heating, (b) fractal principle, (c) 3D modeling for numerical simulation, and (d) boundary conditions used in numerical simulation [101].

**Table 4**  
Mixing performance of passive structures.

Categories	Mixing technique	Mixing index	Reference
Specially designed structure	Curved microchannel	≈ 99%	[29]
	Gear-shaped microchannel	95.8%	[107]
	A string of round cavities in the main channel	≈ 99%	[27]
	Serpentine microchannel with outside bumps	≈ 99%	[112]
Obstacle-based	Sharp corner on one side of the microchannel	88.2%	[113]
	Sharp corner inside the microchannel	90%	[34]
Other distinctive structures	Two-layer structure	90%	[116]
	A quarter of the cross-section of orifices	≈ 99%	[41]



**Fig. 22.** Foci of two elliptic microchannel structures on Y-axis (a) and X-axis (b) [29].

pressure, while delivering a higher mixing efficiency than other curved microchannels, such as zigzag and square-wave structures. This structure can also be combined with other features to further enhance the mixing performance. Fig. 23 shows a similar gear-shaped structure derived by Hong et al. They added some side wells on the two sides of

the main channel in the structure [107]. This structure utilized side wells to produce irregular vortices and fold fluids in a curved channel. Flow disturbance was enhanced dramatically in this structure. Then, the mixing performance of the gear-shaped microchannel and that of the conventional serpentine microchannel at the same flow rate were compared. They set a small and a large flow rate, respectively, to compare the mixing efficiency of the two structures. The results showed that the gear-shaped structure had better mixing performance at both flow rates, indicating that the improved structure can adapt to a larger flow rate range. In addition, the pressure drop ( $\Delta P$ ) between the inlet and outlet of the channel was taken as another parameter indicating the stability of the fluid flow in the channel. This parameter could represent whether the flow is laminar or turbulent. Experimental data showed that after 0.4 mL/min, the gear-shaped channel presented a larger increase in  $\Delta P$ , and this meant that the gear-shaped channel accommodated stronger turbulent flows. The gear-shaped structure could increase the flow rate range for complete mixing, while delivering a higher mixing efficiency (M), which was above 95.8%, than serpentine microchannels. Therefore, this structure achieved improved mixing performance and was utilized to synthesize silica nanoparticles. Specifically, the silica nanoparticles synthesized by this structure had more uniform diameters than those by conventional serpentine channels.

Besides curved microchannel structures, other methods can also be used to abruptly change the cross section of channels for enhanced mixing performance. Dai's research group arranged a string of round cavities in the main channel to enhance the mixing performance, and thus obtained a long-range linear concentration gradient [27]. As shown in Fig. 24, two fluids were injected into the two ends of a T-shape channel, respectively. In this process, a piston made by cured photoresist switched one fluid to replace the other fluid that had filled the entire channel. When the subsequently injected solution entered the cavity, the abruptly enlarged cross section of the microchannel would stretch the fluid to mix with another fluid. According to the experimental results, the process in which the subsequently injected solution replaced the solution in the cavity could go from 10% to 90% in a second. This meant that the mixing efficiency was high enough to facilitate the complete mixing of two solutions. The relationship between the concentration of microdroplets and time was tested, demonstrating that droplets with the target concentration could be obtained at a specific time. The spacing of

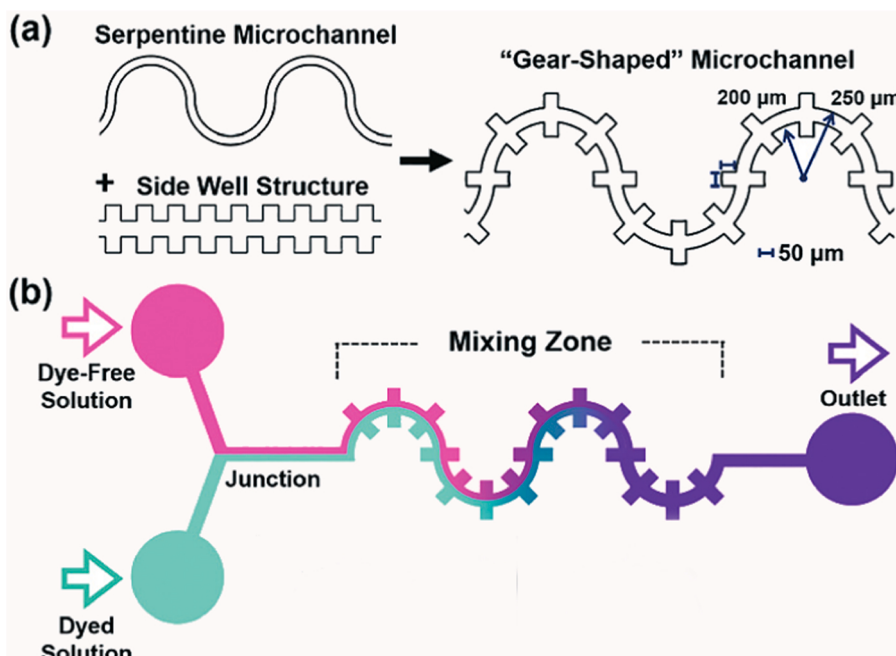


**Fig. 23.** Schematic of a specially designed microchannel [107].

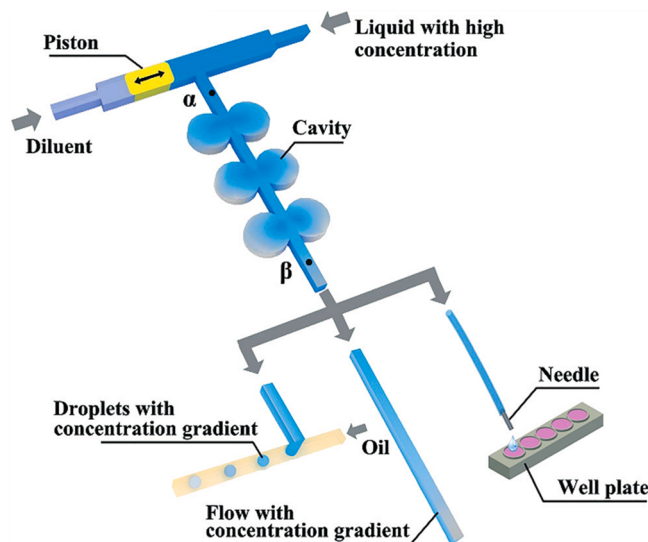


Fig. 24. Schematic of the device and its three representative applications [27].

the particle concentration gradient can be adjusted by changing the flow rate of the side channel. Finally, the reliability of the device was verified by mixing different concentrations of paclitaxel in individual micro-droplets, and 4T1 cells were cultured in a 96-well plate and the micro-droplets were injected one by one into each well. After culturing for 36 h, the cells showed different levels of viability. As mentioned earlier, droplet-based micromixing has received extensive attention because it allows efficient handling of extremely tiny volumes and encapsulating reactions in droplets for different purposes [108]. Due to the symmetrical recirculation vortices appearing in a straight channel, the improvement of the efficiency of droplet-based mixing in passive methods mainly depend on the structure of the microchannel. Therefore, some papers focus on how to promote the mixing efficiency of fluids inside droplets, such as channel height [109], cross-sectional geometry [110], and arrangement of the flow-focusing channel [111]. The basic principle of this method is to study how to enhance the mixing of two-phase reactions in droplets by folding and stretching the droplets. The curved microchannel is the most common used structure. Based on this structure, some obstacles were placed on either side of the micro-channel, as shown in Fig. 25 [112]. In this structure, droplets not only fold and stretch in the serpentine microchannel, but generate an internal chaotic flow at bumps. The final mixing degree of droplets is significantly improved by a centrifugal force, which is enhanced by these bumps. Thus, the symmetrical recirculation vortices are broken in this structure to help realize high mixing performance.

The fluid mixing efficiency can be extremely low in the case of relying on molecular diffusion alone. With obstacle-based structures, some obstacles are arranged in the microchannel to cause a chaotic flow in the fluids, which promotes the mixing efficiency significantly. Among all the existing microchannel structures, the sharp corner is the most

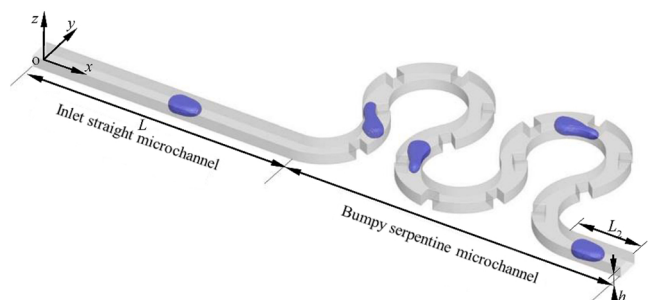


Fig. 25. Geometry of the serpentine channel with several bumps [112].

frequently used obstacle structure. Zhao et al. improved the mixing efficiency of two fluids based on this obstacle-based structure [113]. As shown in Fig. 26, they set up 80 repeated sharp corners on one side of the microchannel, and the angle was designed as the optimal value of 45° based on Zhang's research result [114]. As the flow rate increased, Dean vortices were generated and became stronger at the sharp corner, which improved the fluid mixing efficiency. In addition, they investigated the influence of geometrical characteristics of sharp corners on the mixing performance. It was found that the mixing performance was better when the structure was gradually constricted and suddenly expanded, as shown in Fig. 26(b). In another paper, the researchers conducted an optimization study to improve the mixing efficiency by arranging sharp corners inside the channel [115]. They compared the mixing efficiency of three structures, including a simple arc channel, sharp corners located on one side of the external wall, and sharp corners asymmetrically located on two sides of the external wall. According to simulation and experimental research, although asymmetrically located sharp corners would produce Dean vortices, these vortices can counteract with each other and cause the interface between two fluids to have lower confluence. Sharp corners located on the one side of the external wall turned out to be the most efficient structure among the three. These conclusions provide guidance for the application of sharp-corner obstacle structures. Arranging triangular obstacles in the middle of the channel has a similar effect to arranging sharp corners along the edge of the channel. Zhu et al. combined these two structures together to explore the best way to arrange triangular obstacles inside the microchannel [34]. As shown in Fig. 27, two arrangement schemes were proposed. Although both structures can generate Dean vortices with high flow rate, the transport of fluids in the center toward the edge is another important factor affecting the mixing efficiency. In contrast, asymmetrically placed triangular obstacles can transport more fluids and thereby improve their mixing performance. Such improvement is more significant for fluids with a high  $Re$  than those with a low  $Re$  as turbulence takes place more easily in the former. In addition, through simulation and experiment, it was concluded that the smaller the angle of the sharp base, the more fluids to be transported from the center to the side of the channel, and the better the mixing efficiency.

In addition to the two structures described above, there are some other specially designed structures that feature the advantages of other structures to realize some special functions. However, these structures are not widely used as they involve a complex mold manufacturing process. For example, a two-layer X-crossing channel combine curved and obstacle structures together to improve the mixing performance significantly. Jiang et al. proposed a three-inlet two-layer structure to optimize the performance of multi-component reactions [116]. As shown in Fig. 28, this structure went beyond mixing two side fluids each other by mixing them with the central channel, which was hardly achievable by a normal single-layer structure. On this basis, the researchers compared the influence of  $Re$  on the mixing performance of single-layer and two-layer structures. The mixing efficiency of traditional structures is always below 50%, especially with an increasing  $Re$ . In contrast, two-layer structures can keep the mixing efficiency above 90%, which is slightly influenced by the  $Re$ . One practical application of this structure is the synthesis of Si-based nanoparticles (SiNPs). Two fluids were simultaneously injected into the channel through three inlets, and the final mixing performance was verified by the average diameter of the synthesized SiNPs. Finally, these nanoparticles had a larger mean particle size and a narrower size distribution compared to those synthesized in single-layer structures for mixing three fluids. Another novel structure is a microchannel with baffles inside it. As shown in Fig. 29, the researchers compared three structures with different internal configurations [41]. Through experimental observation, it was found that structure in which a quarter of the cross-section of orifices was covered delivered the highest mixing efficiency. This was because fluids resided in this configuration for the longest period of time. This phenomenon became increasingly prominent with the

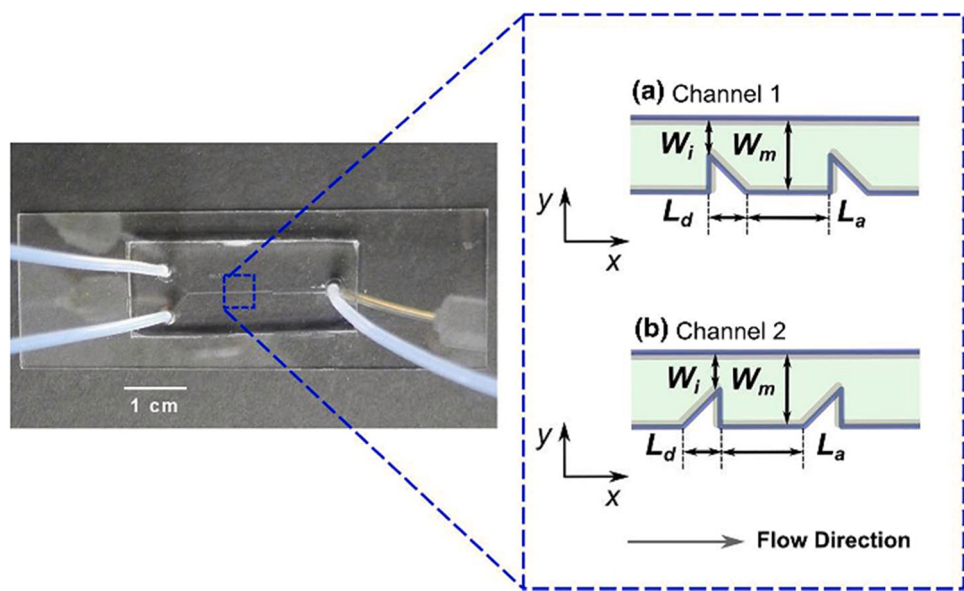


Fig. 26. Schematic of a microchannel with sharp corners [113].

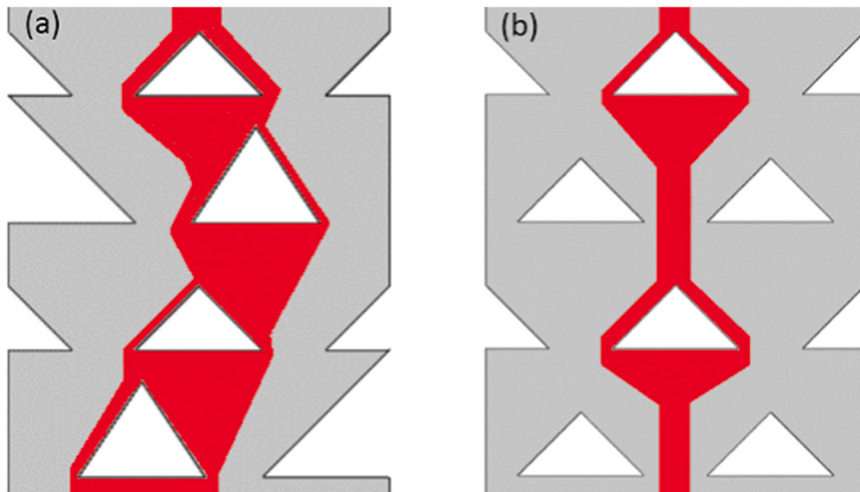


Fig. 27. Schematic of triangular obstacles placed asymmetrically (a) and symmetrically (b) [34].

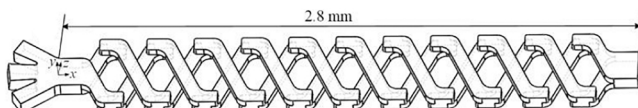


Fig. 28. Structure of a 3D microchannel [116].

increase of  $Re$ . In addition, the increased distance between the baffles would also enhance the mixing performance of these configurations, especially for the third configuration, and the mixing index was as high as 1. The above two representative structures are difficult to manufacture, so the scope of their applicability is limited [15].

### 3. Conclusions and outlook

In recent years, the microfluidic mixing technology has advanced considerably due to its wide application, especially in biological and materials science [117]. However, the rich variety of mixing methods have their own advantages and limitations, so it is important to clearly understand the working principle of each method to identify ideal

methods for different applications. In this review, we provide a state-of-the-art review of the active and passive methods for fluid mixing. Specifically, we divided these methods into five practical active methods and three representative passive methods and compare the difference between them. We gave a detailed discussion on the features of each method, as well as their working principles and practical applications. We also elaborated on the advantages and disadvantages of these methods and summarized ways to improve them, which can be meaningful for the future development of the microfluidic mixing field.

A single method usually cannot provide the desired outcome when it comes to the complex requirements and samples in real-world applications. For example, the synthesis of multi-layer nanoparticles requires a two-step mixing process which is completed in a relatively low length [118]. Huang et al. developed a structure that combined sharp corners with an acoustic field in a single channel, which enabled significantly improved mixing performance and thus more efficient synthesis of these nanoparticles. Therefore, future research on the microfluidic structure for fluid mixing can focus on the combination of different methods. The combination of passive and active methods has been proposed in many previous studies, but the combination of different active methods has

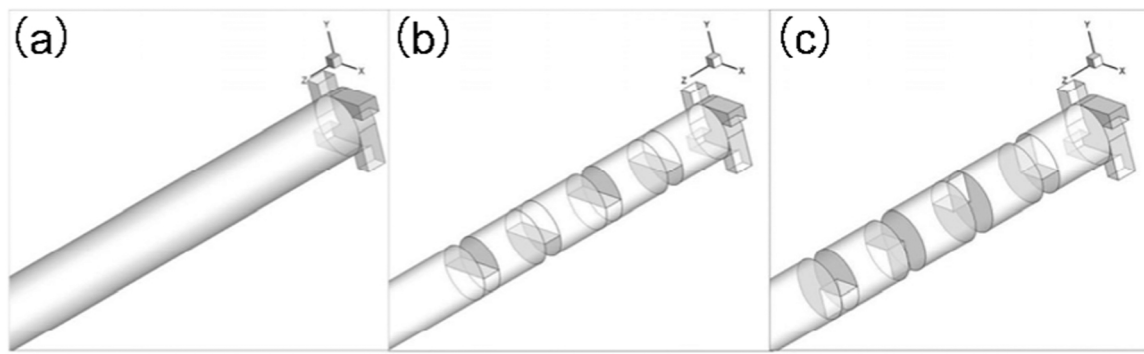


**Fig. 29.** Geometrical illustration of (a) a basic configuration; (b) a configuration with 4 baffles and half cross-sections; (c) a configuration with 4 baffles and quarter cross-sections [41].

been rarely investigated. This idea of combining active methods has been applied in cell separation, and such combinations can be divided into cascaded connections and physical coupling. Cascaded connections include acoustic-electrical [119,120], acoustic-magnetic [121], and electrical-magnetic combinations [122,123], and physical coupling includes acoustic-electrical [124,125] and electrical-magnetic combinations [126,127]. All of these combinations can be used to improve the performance of microfluidic mixing.

Optimizing the chip structure is a way to improve the mixing performance and reduce the consumption of energy. In addition, a reasonable structure can improve the ability of large-scale manufacturing of chips. Recently developed advanced micro-fabrication techniques can help turn a lot of innovation ideas into real products, and soft lithography is the most commonly used technique to fabricate microfluidics chips. The PDMS demolding method is commonly used in the laboratory, but it is not ready for industrial production. In particular, multi-layer structures, however, are difficult to realize [105]. Therefore, further research efforts are required to develop a reliable method that can fabricate precise multi-layer structures. Alternatively, several methods can be combined to reduce the manufacturing complexity and avoid the possibility of manual error. Unlike passive methods, active methods can combine some structures of a passive field to improve the mixing performance, and such combination scheme has been proposed by some studies [69,74,90]. Passive method can also deliver ideal mixing performance in some structures, and they have low requirements for fabrication and manipulation. Hence, to achieve high mixing performance at low costs and requirements, it is essential to explore new schemes that are ready for mass production and can produce reliable results.

Despite their advantages, these methods also have their own limitations, as shown in Table 5. Passive methods deliver lower mixing performance than active methods, which is because it is difficult for fluids with a low  $Re$  usually to produce fluid fluctuations in passive methods. This limitation, however, is not a concern in active methods

[128]. Moreover, the limitation of active method uses different energy inputs and also needs to pay attention. For magnetic-based methods, the need to inject magnetic particles or cilia in advance makes them complex, and the influence of these materials on reagents needs to be considered [71]. Acoustics-based methods have lower costs, but their throughput is unsatisfactory, which limits their application in some fields [42]. Electric-based methods are extremely susceptible to the heat generated within the fluid [129]. Therefore, although external power input can stimulate faster mixing of fluids, but it gives rise to increased temperature of the solution, which is a severe limitation. Thus, some reagents, especially biological cells, are sensitive to temperature and cannot be used in active methods [46]. Passive methods do not require complex structures and power input, and offer an easier and more cost-effective alternative. Complex structures have high requirements for fabrication and are prone to fabrication errors that would cause inaccurate experimental results [103]. In addition, in some complex structures, the channel has the risk of being clogged by some synthetic materials [40]. In contrast, passive methods are less costly and easier to work with, so its scope of applicability is wider than that of active methods. All these methods share one limitation, which is they are not ready for large-scale manufacturing due to challenges with production accuracy and efficiency.

In summary, future studies on microfluidic mixing should be focused on improving the operability and efficiency. First, a feasible approach toward improved mixing efficiency and shorter channel lengths is to combine different methods, including active and passive methods. Combination methods hold great potential for bringing innovative microfluidic mixing ideas into application, especially for those that are still in the proof-of-concept stage. Second, decreasing the requirements for the fabrication and operation of chips is a realistic direction for future researches on microfluidic mixing [130,131]. This direction can help microfluidic mixing chips shift from lab research to real-world applications, and better serve clinical and industrial needs [132]. Third, combining these microfluidic chips with smart devices can reduce errors

**Table 5**  
Summary of mixing methods presented in the review.

Methods	Advantages	Limitations	Suggestion/Comments
Active micromixer			
Magnetic field	Efficient mixing with precise control; versatile	The presence of magnetic materials in samples/reagents; may require multiple stirrers	Concentrate magnetic field strength in small-scale applications
Acoustic field	Nearly instantaneous mixing; easy operation and noninvasiveness	Low throughput; high costs and power consumption	Improve mixing performance by structural innovation
Electric field	Efficient utilization at low voltage; short mixing length	Requires integrated electrodes and conducting liquids; increase the temperature of reagents	Reduce the influence and dependence on conducting liquids
Thermal field	Easy to integrate into a device	Increase the temperature of reagents	Reduce the influence of heaters to samples/reagents
Passive micromixer	Easy operation and simple chip structure; low cost; less effect on reagents	Lower mixing performance	Optimize the chip structure to enhance mixing performance

caused by manual processes [133]. Improved accuracy can greatly improve the reliability of microfluidic chips, and make the microfluidic mixing technology applicable in a wider range of fields. Achieving these ends will enable the microfluidic mixing technology to yield fruitful results.

## Declaration of Competing Interest

The authors declare that they have no known competing financial interests or personal relationships that could have appeared to influence the work reported in this paper.

## Data Availability

Data sharing is not applicable to this article as no new data were created or analyzed in this study.

## Acknowledgment

This work was supported by the National Natural Science Foundation of China (Project Nos. 61973224, 61925307, and 61803323), and the Young Top Talent of Xingliao Program (Project No.: XLYC2007186).

## References

- [1] A.G. Niculescu, C. Chircov, A.C. Bîrcă, A.M. Grumezescu, Fabrication and applications of microfluidic devices: a review, *Int. J. Mol. Sci.* 22 (2021) 1–26, <https://doi.org/10.3390/ijms22042011>.
- [2] C.Y. Lee, L.M. Fu, Recent advances and applications of micromixers, *Sens. Actuators B Chem.* 259 (2018) 677–702, <https://doi.org/10.1016/j.snb.2017.12.034>.
- [3] Y. Mo, G. Rughoobur, A.M.K. Nambiar, K. Zhang, K.F. Jensen, A multifunctional microfluidic platform for high-throughput experimentation of electroorganic chemistry, *Angew. Chem. Int. Ed.* 59 (2020) 20890–20894, <https://doi.org/10.1002/anie.202009819>.
- [4] S. Hu, R. Wang, C.M. Tsang, S.W. Tsao, D. Sun, R.H.W. Lam, Revealing elasticity of largely deformed cells flowing along confining microchannels, *RSC Adv.* 8 (2018) 1030–1038, <https://doi.org/10.1039/c7ra10750a>.
- [5] P. Yager, T. Edwards, E. Fu, K. Helton, K. Nelson, M.R. Tam, B.H. Weigl, Microfluidic diagnostic technologies for global public health, *Nature* 442 (2006) 412–418, <https://doi.org/10.1038/nature05064>.
- [6] J.S. Lee, P. Han, R. Chaudhury, S. Khan, S. Bickerton, M.D. McHugh, H.B. Park, A. L. Siefert, G. Rea, J.M. Carballido, D.A. Horwitz, J. Criscione, K. Perica, R. Samstein, R. Rageb, D. Kim, T.M. Fahmy, Metabolic and immunomodulatory control of type 1 diabetes via orally delivered bile-acid-polymer nanocarriers of insulin or rapamycin, *Nat. Biomed. Eng.* 5 (2021) 983–997, <https://doi.org/10.1038/s41551-021-00791-0>.
- [7] Y. Kawai, T. Yamamoto, Synthesis of dimpled and submicron-sized polymer particles of different morphologies using free micromixer, *Coll. Interface Sci. Commun.* 32 (2019), 100193, <https://doi.org/10.1016/j.colcom.2019.100193>.
- [8] C.K. Chung, T.R. Shih, C.K. Chang, C.W. Lai, B.H. Wu, Design and experiments of a short-mixing-length baffled microreactor and its application to microfluidic synthesis of nanoparticles, *Chem. Eng. J.* 168 (2011) 790–798, <https://doi.org/10.1016/j.cej.2010.12.035>.
- [9] M. Liu, N. Liu, J. Tan, Y. Su, W. Deng, L. Chen, R. Xue, Q. Zhang, Micromixer-assisted Co-precipitation method for fast synthesis of layered Ni-rich materials for lithium-ion batteries, *ChemElectroChem* 6 (2019) 3057–3064, <https://doi.org/10.1002/celec.201900511>.
- [10] M.E. Mäeots, B. Lee, A. Nans, S.G. Jeong, M.M.N. Esfahani, S. Ding, D.J. Smith, C. S. Lee, S.S. Lee, M. Peter, R.I. Enchev, Modular microfluidics enables kinetic insight from time-resolved cryo-EM, *Nat. Commun.* 11 (2020) 1–14, <https://doi.org/10.1038/s41467-020-17230-4>.
- [11] J. Xie, H. Pang, R. Sun, T. Wang, X. Meng, Z. Zhou, Development of rapid and high-precision colorimetric device for organophosphorus pesticide detection based on microfluidic mixer chip, *Micromachines* 12 (2021) 1–13, <https://doi.org/10.3390/mi12030290>.
- [12] P.M. Valencia, P.A. Basto, L. Zhang, M. Rhee, R. Langer, O.C. Farokhzad, R. Karnik, Single-step assembly of homogenous lipid-polymeric and lipid-quantum dot nanoparticles enabled by microfluidic rapid mixing, *ACS Nano* 4 (2010) 1671–1679, <https://doi.org/10.1021/nn901433u>.
- [13] V. Faustino, R.O. Rodrigues, D. Pinho, E. Costa, A. Santos-Silva, V. Miranda, J. S. Amaral, R. Lima, A microfluidic deformability assessment of pathological red blood cells flowing in a hyperbolic converging microchannel, *Micromachines* 10 (2019), <https://doi.org/10.3390/mi10100645>.
- [14] S.Y. Yang, F.Y. Cheng, C.S. Yeh, G. Bin Lee, Size-controlled synthesis of gold nanoparticles using a micro-mixing system, *Microfluid. Nanofluidics* 8 (2010) 303–311, <https://doi.org/10.1007/s10404-009-0461-2>.
- [15] S. Vyawahare, M. Brundage, A. Kijac, M. Gutierrez, M. De Geus, S. Sinha, Sorting droplets into many outlets †, 2021, 1–11.
- [16] S.G. De Pedro, C.S. Martínez-Cisneros, M. Puyol, J. Alonso-Chamarro, Microreactor with integrated temperature control for the synthesis of CdSe nanocrystals, *Lab Chip* 12 (2012) 1979–1986, <https://doi.org/10.1039/c2lc00011c>.
- [17] Z. Liu, F. Fontana, A. Python, J.T. Hirvonen, H.A. Santos, Microfluidics for production of particles: mechanism, methodology, and applications, *Small* 16 (2020) 1–24, <https://doi.org/10.1002/smll.201904673>.
- [18] H.C. Choi, Y.M. Jung, S. Bin Kim, Size effects in the Raman spectra of TiO<sub>2</sub> nanoparticles, *Vib. Spectrosc.* 37 (2005) 33–38, <https://doi.org/10.1016/j.vibspec.2004.05.006>.
- [19] B.X. Wang, L.P. Zhou, X.F. Peng, Surface and size effects on the specific heat capacity of nanoparticles, *Int. J. Thermophys.* 27 (2006) 139–151, <https://doi.org/10.1007/s10765-006-0022-9>.
- [20] R. Reske, H. Mistry, F. Behafarid, B. Roldan Cuanya, P. Strasser, Particle size effects in the catalytic electroreduction of CO<sub>2</sub> on Cu nanoparticles, *J. Am. Chem. Soc.* 136 (2014) 6978–6986, <https://doi.org/10.1021/ja500328k>.
- [21] H.B. Fu, J.N. Yao, Size effects on the optical properties of organic nanoparticles, *J. Am. Chem. Soc.* 123 (2001) 1434–1439, <https://doi.org/10.1021/ja0026298>.
- [22] J. Wu, S. Ma, M. Li, X. Hu, N. Jiao, S. Tung, L. Liu, Enzymatic/magnetic hybrid micromotors for synergistic anticancer therapy, *ACS Appl. Mater. Interfaces* 13 (2021) 31514–31526, <https://doi.org/10.1021/acsami.1c07593>.
- [23] I.O. De Solorzano, L. Uson, A. Larrea, M. Miana, V. Sebastian, M. Arruebo, Continuous synthesis of drug-loaded nanoparticles using microchannel emulsification and numerical modeling: effect of passive mixing, *Int. J. Nanomed.* 11 (2016) 3397–3416, <https://doi.org/10.2147/IJN.S108812>.
- [24] F. Tang, L. Li, D. Chen, Mesoporous silica nanoparticles: synthesis, biocompatibility and drug delivery, *Adv. Mater.* 24 (2012) 1504–1534, <https://doi.org/10.1002/adma.201104763>.
- [25] L. Frenz, A. El Harrak, M. Pauly, S. Bégin-Colin, A.D. Griffiths, J.C. Baret, Droplet-based microreactors for the synthesis of magnetic iron oxide nanoparticles, *Angew. Chem. Int. Ed.* 47 (2008) 6817–6820, <https://doi.org/10.1002/anie.200801360>.
- [26] R. Karnik, F. Gu, P. Basto, C. Cannizzaro, L. Dean, W. Kyei-manu, R. Langer, O.C. Farokhzad, Microfluidic Platform for Controlled Synthesis of Polymeric Nanoparticles, 2008.
- [27] B. Dai, Y. Long, J. Wu, S. Huang, Y. Zhao, L. Zheng, C. Tao, S. Guo, F. Lin, Y. Fu, D. Zhang, S. Zhuang, Generation of flow and droplets with an ultra-long-range linear concentration gradient, *Lab Chip* (2021), <https://doi.org/10.1039/d1lc00749a>.
- [28] (and) X.Z.L. Capretto, W. Cheng, M. Hill, Micromixing within microfluidic devices, *Pept. Mater.* 310 (2011) 1–26, <https://doi.org/10.1007/128>.
- [29] X. Wang, Z. Liu, Y. Cai, B. Wang, X. Luo, A cost-effective serpentine micromixer utilizing ellipse curve, *Anal. Chim. Acta* 1155 (2021), <https://doi.org/10.1016/j.aca.2021.338355>.
- [30] M. Serhan, M. Sprowls, D. Jackemeyer, M. Long, I.D. Perez, W. Maret, N. Tao, E. Forzani, Total iron measurement in human serum with a smartphone, *AIChE Annu. Meet. Conf. Proc.* 2019-Novem, 2019. <https://doi.org/10.1039/x0xx00000x>.
- [31] C.-C. Chen, P.H. Diamond, Potential vorticity mixing in a tangled magnetic field, *Astrophys. J.* 892 (2020) 24, <https://doi.org/10.3847/1538-4357/ab774f>.
- [32] J. Nam, C.S. Lim, Micromixing using swirling induced by three-dimensional dual surface acoustic waves (3D-dSAW), *Sens. Actuators, B Chem.* 255 (2018) 3434–3440, <https://doi.org/10.1016/j.snb.2017.09.173>.
- [33] Y. Ren, W. Liu, Y. Tao, M. Hui, Q. Wu, On AC-field-induced nonlinear electroosmosis next to the sharp corner-field-singularity of leaky dielectric blocks and its application in on-chip micro-mixing, *Micromachines* 9 (2018), <https://doi.org/10.3390/mi9030102>.
- [34] K. Chen, H. Lu, M. Sun, L. Zhu, Y. Cui, Mixing enhancement of a novel C-SAR microfluidic mixer, *Chem. Eng. Res. Des.* 132 (2018) 338–345, <https://doi.org/10.1016/j.cherd.2018.01.032>.
- [35] A. Gu, M. Jhunjhunwala, M. Thalmann, M.A. Schmidt, K.F. Jensen, La0482406. Pdf, 2005, 1547–1555.
- [36] G.G. Yaralioglu, I.O. Wygant, T.C. Marentis, B.T. Khuri-Yakub, Ultrasonic mixing in microfluidic channels using integrated transducers, *Anal. Chem.* 76 (2004) 3694–3698, <https://doi.org/10.1021/ac035220k>.
- [37] S. Hardt, F. Schönfeld, Laminar mixing in different interdigital micromixers: II. Numerical simulations, *AIChE J.* 49 (2003) 578–584, <https://doi.org/10.1002/aic.690490305>.
- [38] Y. Li, C. Liu, X. Feng, Y. Xu, B.F. Liu, Ultrafast microfluidic mixer for tracking the early folding kinetics of human telomere G-quadruplex, *Anal. Chem.* 86 (2014) 4333–4339, <https://doi.org/10.1021/ac500112d>.
- [39] F. Tian, L. Cai, C. Liu, J. Sun, Microfluidic technologies for nanoparticle formation, *Lab Chip* 22 (2022) 512–529, <https://doi.org/10.1039/d1lc00812a>.
- [40] W. Raza, S. Hossain, K.Y. Kim, Effective Mixing in A Short Serpentine Split-and-recombination Micromixer, *Elsevier B.V.* 2018, <https://doi.org/10.1016/j.snb.2017.11.135>.
- [41] R. Milotin, D. Lelea, The passive mixing phenomena in microtubes with baffle configuration, *Procedia Technol.* 22 (2016) 243–250, <https://doi.org/10.1016/j.prot.2016.01.075>.
- [42] S.A. Endayalalu, W.H. Tien, Mixing enhancement in T-junction microchannel with acoustic streaming induced by triangular structure, *Biomicrofluidics* 15 (2021), <https://doi.org/10.1063/5.0042541>.
- [43] A.J. DeMello, Control and detection of chemical reactions in microfluidic systems, *Nature* 442 (2006) 394–402, <https://doi.org/10.1038/nature05062>.

- [44] K. Illath, S. Kar, P. Gupta, A. Shinde, S. Wankhar, F.G. Tseng, K.T. Lim, M. Nagai, T.S. Santra, Microfluidic nanomaterials: from synthesis to biomedical applications, *Biomaterials* 280 (2022), 121247, <https://doi.org/10.1016/j.biomaterials.2021.121247>.
- [45] Y. Liu, X. Jiang, Why microfluidics? Merits and trends in chemical synthesis, *Lab Chip* 17 (2017) 3960–3978, <https://doi.org/10.1039/c7lc00627f>.
- [46] K. Ward, Z.H. Fan, Mixing in microfluidic devices and enhancement methods, *J. Micromech. Microeng.* 25 (2015) 94001, <https://doi.org/10.1088/0960-1317/25/9/094001>.
- [47] C.Y. Lee, C.L. Chang, Y.N. Wang, L.M. Fu, Microfluidic mixing: a review, *Int. J. Mol. Sci.* 12 (2011) 3263–3287, <https://doi.org/10.3390/ijms12053263>.
- [48] S.H. Lee, D. Van Noort, J.Y. Lee, B.T. Zhang, T.H. Park, Effective mixing in a microfluidic chip using magnetic particles, *Lab Chip* 9 (2009) 479–482, <https://doi.org/10.1039/b814371d>.
- [49] C.Y. Wen, C.P. Yeh, C.H. Tsai, L.M. Fu, Rapid magnetic microfluidic mixer utilizing AC electromagnetic field, *Electrophoresis* 30 (2009) 4179–4186, <https://doi.org/10.1002/elps.200900400>.
- [50] G.P. Zhu, N.T. Nguyen, Rapid magnetofluidic mixing in a uniform magnetic field, *Lab Chip* 12 (2012) 4772–4780, <https://doi.org/10.1039/c2lc40818j>.
- [51] M. Hejazian, N.T. Nguyen, A rapid magnetofluidic micromixer using diluted ferrofluid, *Micromachines* 8 (2017), <https://doi.org/10.3390/mi8020037>.
- [52] G. Kitenberg, K. Erglis, R. Perzynski, A. Cébers, Magnetic particle mixing with magnetic micro-convection for microfluidics, *J. Magn. Magn. Mater.* 380 (2015) 227–230, <https://doi.org/10.1016/j.jmmm.2014.10.033>.
- [53] C.Y. Chen, C.Y. Chen, C.Y. Lin, Y.T. Hu, Magnetically actuated artificial cilia for optimum mixing performance in microfluidics, *Lab Chip* 13 (2013) 2834–2839, <https://doi.org/10.1039/c3lc50407g>.
- [54] J.E. Martin, L. Shea-Rohwer, K.J. Solis, Strong intrinsic mixing in vortex magnetic fields, *Phys. Rev. E Stat. Nonlinear Soft Matter Phys.* 80 (2009) 1–6, <https://doi.org/10.1103/PhysRevE.80.016312>.
- [55] F. Wittbracht, A. Weddemann, B. Eickenberg, M. Zahn, A. Hüttner, Enhanced fluid mixing and separation of magnetic bead agglomerates based on dipolar interaction in rotating magnetic fields, *Appl. Phys. Lett.* 100 (2012), <https://doi.org/10.1063/1.3696886>.
- [56] J. Den Toonder, F. Bos, D. Broer, L. Filippini, M. Gillies, J. De Goede, T. Mol, M. Reijme, W. Talen, H. Wilderbeek, V. Khatavkar, P. Anderson, Artificial cilia for active microfluidic mixing, *Lab Chip* 8 (2008) 533–541, <https://doi.org/10.1039/b717681c>.
- [57] Y. Gao, A. Van Reenen, M.A. Hulsen, A.M. De Jong, M.W.J. Prins, J.M.J. Den Toonder, Chaotic fluid mixing by alternating microparticle topologies to enhance biochemical reactions, *Microfluid. Nanofluidics* 16 (2014) 265–274, <https://doi.org/10.1007/s10404-013-1209-6>.
- [58] M. Rahbar, L. Shannon, B.L. Gray, Microfluidic active mixers employing ultra-high aspect-ratio rare-earth magnetic nano-composite polymer artificial cilia, *J. Micromech. Microeng.* 24 (2014), <https://doi.org/10.1088/0960-1317/24/2/025003>.
- [59] D. Nouri, A. Zabihi-Hesari, M. Passandideh-Fard, Rapid mixing in micromixers using magnetic field, *Sens. Actuators A Phys.* 255 (2017) 79–86, <https://doi.org/10.1016/j.sna.2017.01.005>.
- [60] A. Munaz, H. Kamble, M.J.A. Shiddiky, N.T. Nguyen, Magnetofluidic micromixer based on a complex rotating magnetic field, *RSC Adv.* 7 (2017) 52465–52474, <https://doi.org/10.1039/c7ra08073e>.
- [61] Q. Cao, X. Han, L. Li, An active microfluidic mixer utilizing a hybrid gradient magnetic field, *Int. J. Appl. Electromagn. Mech.* 47 (2015) 583–592, <https://doi.org/10.3233/JAE-140057>.
- [62] R. Zhou, A.N. Surendran, M. Mejulu, Y. Lin, Rapid microfluidic mixer based on ferrofluid and integrated microscale ndfeb-pdms magnet, *Micromachines* 11 (2020) 1–16, <https://doi.org/10.3390/mi11010029>.
- [63] R. Zhou, A. Surendran, J. Wang, Fabrication and characteristic study on mixing enhancement of a magnetofluidic mixer, *Sens. Actuators A Phys.* 326 (2021), 112733, <https://doi.org/10.1016/j.sna.2021.112733>.
- [64] R. Zhou, A.N. Surendran, Study on micromagnets induced local wavy mixing in a microfluidic channel, *Appl. Phys. Lett.* 117 (2020), <https://doi.org/10.1063/5.0024011>.
- [65] F. Liu, J. Zhang, G. Alici, S. Yan, R. Mutlu, W. Li, T. Yan, An inverted micro-mixer based on a magnetically-actuated cilium made of Fe doped PDMS, *Smart Mater. Struct.* 25 (2016) 1–7, <https://doi.org/10.1088/0964-1726/25/9/095049>.
- [66] Y.A. Wu, B. Panigrahi, C.Y. Chen, Hydrodynamically efficient micropropulsion through a new artificial cilia beating concept, *Microsyst. Technol.* 23 (2017) 5893–5902, <https://doi.org/10.1007/s00542-017-3428-3>.
- [67] E.S. Shanko, L. Ceelen, Y. Wang, Y. van de Burgt, J. den Toonder, Enhanced microfluidic sample homogeneity and improved antibody-based assay kinetics due to magnetic mixing, *ACS Sens.* 6 (2021) 2553–2562, <https://doi.org/10.1021/acssens.1c00050>.
- [68] B. Zhou, W. Xu, A.A. Syed, Y. Chau, L. Chen, B. Chew, O. Yassine, X. Wu, Y. Gao, J. Zhang, X. Xiao, J. Kosei, X.X. Zhang, Z. Yao, W. Wen, Design and fabrication of magnetically functionalized flexible micropillar arrays for rapid and controllable microfluidic mixing, *Lab Chip* 15 (2015) 2125–2132, <https://doi.org/10.1039/c5lc00173k>.
- [69] R.E. Pawinanto, J. Yunas, A.M. Hashim, Design optimization of active microfluidic mixer incorporating micropillar on flexible membrane, *Microsyst. Technol.* 25 (2019) 1203–1209, <https://doi.org/10.1007/s00542-018-4134-5>.
- [70] W.H. Chong, Y. Huang, T.N. Wong, K.T. Ooi, G.P. Zhu, Magnetic nanorobots, generating vortexes inside nanoliter droplets for effective mixing, *Adv. Mater. Technol.* 3 (2018) 1–7, <https://doi.org/10.1002/admt.201700312>.
- [71] G. Chen, B. Ji, Y. Gao, C. Wang, J. Wu, B. Zhou, W. Wen, Towards the rapid and efficient mixing on “open-surface” droplet-based microfluidics via magnetic actuation, *Sens. Actuators B Chem.* 286 (2019) 181–190, <https://doi.org/10.1016/j.snb.2019.01.126>.
- [72] P.H. Huang, Y. Xie, D. Ahmed, J. Rufo, N. Nama, Y. Chen, C.Y. Chan, T.J. Huang, An acoustofluidic micromixer based on oscillating sidewall sharp-edges, *Lab Chip* 13 (2013) 3847–3852, <https://doi.org/10.1039/c3lc50568e>.
- [73] N. Nama, P.H. Huang, T.J. Huang, F. Costanzo, Investigation of micromixing by acoustically oscillated sharp-edges, *Biomicrofluidics* 10 (2016) 1–17, <https://doi.org/10.1063/1.4946875>.
- [74] C. Zhang, P. Brunet, L. Royon, X. Guo, Mixing intensification using sound-driven micromixer with sharp edges, *Chem. Eng. J.* 410 (2021), 128252, <https://doi.org/10.1016/j.cej.2020.128252>.
- [75] H. Bachman, C. Chen, J. Rufo, S. Zhao, S. Yang, Z. Tian, N. Nama, P.H. Huang, T. J. Huang, An acoustofluidic device for efficient mixing over a wide range of flow rates, *Lab Chip* 20 (2020) 1238–1248, <https://doi.org/10.1039/c9lc01171d>.
- [76] A. Hashmi, G. Yu, M. Reilly-Collette, G. Heiman, J. Xu, Oscillating bubbles: a versatile tool for lab on a chip applications, *Lab Chip* 12 (2012) 4216–4227, <https://doi.org/10.1039/c2lc40424a>.
- [77] M.R. Rasouli, M. Tabrizian, An ultra-rapid acoustic micromixer for synthesis of organic nanoparticles, *Lab Chip* 19 (2019) 3316–3325, <https://doi.org/10.1039/c9lc00637k>.
- [78] N.H.A. Le, H. Van Phan, J. Yu, H.K. Chan, A. Neild, T. Alan, Acoustically enhanced microfluidic mixer to synthesize highly uniform nanodrugs without the addition of stabilizers, *Int. J. Nanomed.* 13 (2018) 1353–1359, <https://doi.org/10.2147/IJN.S153805>.
- [79] N.H. An Le, H. Deng, C. Devendran, N. Akhtar, X. Ma, C. Pouton, H.K. Chan, A. Neild, T. Alan, Ultrafast star-shaped acoustic micromixer for high throughput nanoparticle synthesis, *Lab Chip* 20 (2020) 582–591, <https://doi.org/10.1039/c9lc01174a>.
- [80] H. Ahmed, J. Park, G. Destgeer, M. Afzal, H.J. Sung, Surface acoustic wave-based micromixing enhancement using a single interdigital transducer, *Appl. Phys. Lett.* 114 (2019), <https://doi.org/10.1063/1.5079815>.
- [81] H. Lim, S.M. Back, H. Choi, J. Nam, Acoustic mixing in a dome-shaped chamber-based SAW (DC-SAW) device, *Lab Chip* 20 (2020) 120–125, <https://doi.org/10.1039/c9lc00820a>.
- [82] J. Castro, S. Ramesan, A. Rezk, L. Yeo, *Continuous tuneable droplet ejection via pulsed*, *Soft Matter* (2018).
- [83] D. Ashtiani, H. Venugopal, M. Belousov, B. Spicer, J. Mak, A. Neild, A. de Marco, Delivery of femtolitre droplets using surface acoustic wave based atomisation for cryo-EM grid preparation, *J. Struct. Biol.* 203 (2018) 94–101, <https://doi.org/10.1016/j.jsb.2018.03.012>.
- [84] Y. Zhang, C. Devendran, C. Lupton, A. De Marco, A. Neild, Versatile platform for performing protocols on a chip utilizing surface acoustic wave (SAW) driven mixing, *Lab Chip* 19 (2019) 262–271, <https://doi.org/10.1039/c8LC01117F>.
- [85] C. Pothuri, M. Azharudeen, K. Subramani, Rapid mixing in microchannel using standing bulk acoustic waves, *Phys. Fluids* 31 (2019), <https://doi.org/10.1063/1.5126259>.
- [86] M. Viehues, R. Eichhorn, E. Fredrich, J. Regtmeier, D. Anselmetti, Continuous and reversible mixing or demixing of nanoparticles by dielectrophoresis, *Lab Chip* 12 (2012) 485–494, <https://doi.org/10.1039/c1lc20610a>.
- [87] K. Zhang, Y. Ren, L. Hou, X. Feng, X. Chen, H. Jiang, An efficient micromixer actuated by induced-charge electroosmosis using asymmetrical floating electrodes, *Microfluid. Nanofluidics* 22 (2018) 0, <https://doi.org/10.1007/s10404-018-2153-2>.
- [88] M. Nazari, S. Rashidi, J.A. Esfahani, Mixing process and mass transfer in a novel design of induced-charge electrokinetic micromixer with a conductive mixing-chamber, *Int. Commun. Heat. Mass Transf.* 108 (2019), 104293, <https://doi.org/10.1016/j.icheatmastransfer.2019.104293>.
- [89] P. Modarres, M. Tabrizian, Phase-controlled field-effect micromixing using AC electroosmosis, *Microsyst. Nanoeng.* 6 (2020), <https://doi.org/10.1038/s41378-020-0166-y>.
- [90] S. Najjaran, S. Rashidi, M.S. Valipour, A new design of induced-charge electrokinetic micromixer with corrugated walls and conductive plate installation, *Int. Commun. Heat. Mass Transf.* 114 (2020), 104564, <https://doi.org/10.1016/j.icheatmastransfer.2020.104564>.
- [91] Z. Wu, X. Chen, Numerical simulation of a novel microfluidic electroosmotic micromixer with Cantor fractal structure, *Microsyst. Technol.* 25 (2019) 3157–3164, <https://doi.org/10.1007/s00542-019-04311-8>.
- [92] S. Xiong, X. Chen, Numerical study of a three-dimensional electroosmotic micromixer with Koch fractal curve structure, *J. Chem. Technol. Biotechnol.* 96 (2021) 1909–1917, <https://doi.org/10.1002/jctb.6711>.
- [93] A. Usefian, M. Bayareh, A. Shateri, N. Taheri, Numerical study of electro-osmotic micro-mixing of Newtonian and non-Newtonian fluids, *J. Braz. Soc. Mech. Sci. Eng.* 41 (2019) 1–10, <https://doi.org/10.1007/s40430-019-1739-2>.
- [94] Y. Xing, Y. Liu, R. Chen, Y. Li, C. Zhang, Y. Jiang, Y. Lu, B. Lin, P. Chen, R. Tian, X. Liu, X. Cheng, A robust and scalable active-matrix driven digital microfluidic platform based on printed-circuit board technology, *Lab Chip* 21 (2021) 1886–1896, <https://doi.org/10.1039/c1lc00101a>.
- [95] J. Yu, X. Wei, Y. Guo, Z. Zhang, P. Rui, Y. Zhao, W. Zhang, S. Shi, P. Wang, Self-powered droplet manipulation system for microfluidics based on triboelectric nanogenerator harvesting rotary energy, *Lab Chip* 21 (2021) 284–295, <https://doi.org/10.1039/dlc00994f>.
- [96] D. Ding, X. Zhong, B. Liu, L. Shi, T. Zhou, Y. Zhu, Mixing mechanism of a straight channel micromixer based on light-actuated oscillating electroosmosis in low-

- frequency sinusoidal AC electric field, *Microfluid. Nanofluidics* 25 (2021) 1–15, <https://doi.org/10.1007/s10404-021-02430-1>.
- [97] J.H. Tsai, L. Lin, Active microfluidic mixer and gas bubble filter driven by thermal bubble micropump, *Sens. Actuators A Phys.* 97–98 (2002) 665–671, [https://doi.org/10.1016/S0924-4247\(02\)00031-6](https://doi.org/10.1016/S0924-4247(02)00031-6).
- [98] F. Zhang, H. Chen, B. Chen, J. Wu, Alternating current electrothermal micromixer with thin film resistive heaters, *Adv. Mech. Eng.* 8 (2016) 1–10, <https://doi.org/10.1177/1687814016646264>.
- [99] A. Khakpour, A. Ramiar, Numerical investigation of the effect of electrode arrangement and geometry on electrothermal fluid flow pumping and mixing in microchannel, *Chem. Eng. Process. Process. Intensif.* 150 (2020), 107864, <https://doi.org/10.1016/j.cep.2020.107864>.
- [100] H. Lv, X. Chen, New insights into the mechanism of fluid mixing in the micromixer based on alternating current electric heating with film heaters, *Int. J. Heat. Mass Transf.* 181 (2021), 121902, <https://doi.org/10.1016/j.ijheattransfer.2021.121902>.
- [101] H. Lv, X. Chen, X. Li, Y. Ma, D. Zhang, Finding the optimal design of a Cantor fractal-based AC electric micromixer with film heating sheet by a three-objective optimization approach, *Int. Commun. Heat. Mass Transf.* 131 (2022), 105867, <https://doi.org/10.1016/j.icheatmasstransfer.2021.105867>.
- [102] K. Zhang, Y. Ren, L. Hou, Y. Tao, W. Liu, T. Jiang, H. Jiang, Continuous microfluidic mixing and the highly controlled nanoparticle synthesis using direct current-induced thermal buoyancy convection, *Microfluid. Nanofluidics* 24 (2020), <https://doi.org/10.1007/s10404-019-2306-y>.
- [103] C. Chen, Y. Zhao, J. Wang, P. Zhu, Y. Tian, M. Xu, L. Wang, X. Huang, Passive mixing inside microdroplets, *Micromachines* 9 (2018) 1–16, <https://doi.org/10.3390/mi9040160>.
- [104] X. Chen, S. Zhang, Z. Wu, Y. Zheng, A novel Koch fractal micromixer with rounding corners structure, *Microsyst. Technol.* 25 (2019) 2751–2758, <https://doi.org/10.1007/s00542-019-04296-4>.
- [105] A.P. Sudarsan, V.M. Ugar, Fluid mixing in planar spiral microchannels, *Lab Chip* 6 (2005) 74–82, <https://doi.org/10.1039/b511524h>.
- [106] S. Baheri Islami, M. Khezerloo, Enhancement of mixing performance of non-newtonian fluids using curving and grooving of microchannels, *J. Appl. Fluid Mech.* 10 (2017) 127–141, <https://doi.org/10.18869/acadpub.jafm.73.238.26374>.
- [107] S.O. Hong, K.S. Park, D.Y. Kim, S.S. Lee, C.S. Lee, J.M. Kim, Gear-shaped micromixer for synthesis of silica particles utilizing inertio-elastic flow instability, *Lab Chip* 21 (2021) 513–520, <https://doi.org/10.1039/d0lc00834f>.
- [108] X. Casadevall i Solvas, A. De Mello, Droplet microfluidics: recent developments and future applications, *Chem. Commun.* 47 (2011) 1936–1942, <https://doi.org/10.1039/c0cc02474k>.
- [109] O. Kašpar, A.H. Koyuncu, A. Hubatová-Vacková, M. Balouch, V. Tokárová, Influence of channel height on mixing efficiency and synthesis of iron oxide nanoparticles using droplet-based microfluidics, *RSC Adv.* 10 (2020) 15179–15189, <https://doi.org/10.1039/d0ra02470h>.
- [110] E. Ghazimirsaeed, M. Madadelahi, M. Dizani, A. Shamloo, Secondary flows, mixing, and chemical reaction analysis of droplet-based flow inside serpentine microchannels with different cross sections, *Langmuir* 37 (2021) 5118–5130, <https://doi.org/10.1021/acs.langmuir.0c03662>.
- [111] K.I. Belousov, N.A. Filatov, I.V. Kukhovich, V. Kantsler, A.A. Evstratov, A. S. Bukatin, An asymmetric flow-focusing droplet generator promotes rapid mixing of reagents, *Sci. Rep.* 11 (2021), <https://doi.org/10.1038/s41598-021-88174-y>.
- [112] X. Cao, B. Zhou, C. Yu, X. Liu, Droplet-based mixing characteristics in bumpy serpentine microchannel, *Chem. Eng. Process. - Process. Intensif.* 159 (2021), 108246, <https://doi.org/10.1016/j.cep.2020.108246>.
- [113] L.L. Fan, X.L. Zhu, H. Zhao, J. Zhe, L. Zhao, Rapid microfluidic mixer utilizing sharp corner structures, *Microfluid. Nanofluidics* 21 (2017) 1–12, <https://doi.org/10.1007/s10404-017-1874-y>.
- [114] Y. Zhang, Y. Hu, H. Wu, Design and simulation of passive micromixers based on capillary, *Microfluid. Nanofluidics* 13 (2012) 809–818, <https://doi.org/10.1007/s10404-012-1002-y>.
- [115] L.R. Huang, L.L. Fan, Q. Liu, Z. Zhao, J. Zhe, L. Zhao, Enhancement of passive mixing via arc microchannel with sharp corner structure, *J. Micromech. Microeng.* 31 (2021) 1–11, <https://doi.org/10.1088/1361-6439/abf334>.
- [116] X. Feng, Y. Ren, L. Hou, Y. Tao, T. Jiang, W. Li, H. Jiang, Tri-fluid mixing in a microchannel for nanoparticle synthesis, *Lab Chip* 19 (2019) 2936–2946, <https://doi.org/10.1039/c9lc00425d>.
- [117] E.A. Mansur, M. YE, Y. WANG, Y. DAI, A state-of-the-art review of mixing in microfluidic mixers, *Chin. J. Chem. Eng.* 16 (2008) 503–516, [https://doi.org/10.1016/S1004-9541\(08\)60114-7](https://doi.org/10.1016/S1004-9541(08)60114-7).
- [118] S. Zhao, P.H. Huang, H. Zhang, J. Rich, H. Bachman, J. Ye, W. Zhang, C. Chen, Z. Xie, Z. Tian, P. Kang, H. Fu, T.J. Huang, Fabrication of tunable, high-molecular-weight polymeric nanoparticles via ultrafast acoustofluidic micromixing, *Lab Chip* 21 (2021) 2453–2463, <https://doi.org/10.1039/d1lc00265a>.
- [119] S.K. Ravula, D.W. Branch, C.D. James, R.J. Townsend, M. Hill, G. Kaduchak, M. Ward, I. Brener, A microfluidic system combining acoustic and dielectrophoretic particle preconcentration and focusing, *Sens. Actuators B Chem.* 130 (2008) 645–652, <https://doi.org/10.1016/j.snb.2007.10.024>.
- [120] B. Çetin, M.B. Özer, E. Çağatay, S. Büyükköçak, An integrated acoustic and dielectrophoretic particle manipulation in a microfluidic device for particle wash and separation fabricated by mechanical machining, *Biomicrofluidics* 10 (2016), <https://doi.org/10.1063/1.4940431>.
- [121] J.D. Adams, P. Thvoz, H. Bruus, H.T. Soh, Integrated acoustic and magnetic separation in microfluidic channels, *Appl. Phys. Lett.* 95 (2009), <https://doi.org/10.1063/1.3275577>.
- [122] U. Kim, H.T. Soh, Simultaneous sorting of multiple bacterial targets using integrated Dielectrophoretic / Magnetic Activated Cell Sorter, *Proc. Conf. MicroTAS 2009 - 13th Int. Conf. Miniaturized Syst. Chem. Life Sci.* (2009) 1898–1900.
- [123] J.N. Krishnan, C. Kim, H.J. Park, J.Y. Kang, T.S. Kim, S.K. Kim, Rapid microfluidic separation of magnetic beads through dielectrophoresis and magnetophoresis, *Electrophoresis* 30 (2009) 1457–1463, <https://doi.org/10.1002/elps.200800646>.
- [124] M. Tayebi, D. Yang, D.J. Collins, Y. Ai, Deterministic sorting of submicrometer particles and extracellular vesicles using a combined electric and acoustic field, *Nano Lett.* 21 (2021) 6835–6842, <https://doi.org/10.1021/acs.nanolett.1c01827>.
- [125] M. Wiklund, C. Günther, R. Lemor, M. Jäger, G. Fuhr, H.M. Hertz, Ultrasonic standing wave manipulation technology integrated into a dielectrophoretic chip, *Lab Chip* 6 (2006) 1537–1544, <https://doi.org/10.1039/b612064b>.
- [126] D. Issadore, T. Franke, K.A. Brown, T.P. Hunt, R.M. Westervelt, High-voltage dielectrophoretic and magnetophoretic hybrid integrated circuit/microfluidic chip, *J. Micro. Syst.* 18 (2009) 1220–1225, <https://doi.org/10.1109/JMEMS.2009.2030422>.
- [127] C.D. James, J. McClain, K.R. Pohl, N. Reuel, K.E. Achyuthan, C.J. Bourdon, K. Rahimian, P.C. Galambos, G. Ludwig, M.S. Derzon, High-efficiency magnetic particle focusing using dielectrophoresis and magnetophoresis in a microfluidic device, *J. Micromech. Microeng.* 20 (2010), <https://doi.org/10.1088/0960-1317/20/4/045015>.
- [128] X. Huanming, W. Jiawei, W. Zhiping, A comparative discussion of different designs of passive micromixers: specific sensitivities of mixing efficiency on Reynolds numbers and fluid properties, *Microsyst. Technol.* 24 (2018) 1253–1263, <https://doi.org/10.1007/s00542-017-3496-4>.
- [129] H. Mirzajani, C. Cheng, J. Wu, C.S. Ivanoff, E. Najafi Aghdam, H. Badri Ghavifekr, Design and characterization of a passive, disposable wireless AC-electroosmotic lab-on-a-film for particle and fluid manipulation, *Sens. Actuators B Chem.* 235 (2016) 330–342, <https://doi.org/10.1016/j.snb.2016.05.073>.
- [130] T. Ghonge, H. Ceylan Koydemir, E. Valera, J. Berger, C. Garcia, N. Nawar, J. Tiao, G.L. Damhorst, A. Ganguli, U. Hassan, A. Ozcan, R. Bashir, Smartphone-imaged microfluidic biochip for measuring CD64 expression from whole blood, *Analyst* 144 (2019) 3925–3935, <https://doi.org/10.1039/c9an00532c>.
- [131] S. Dudala, S.K. Dubey, S. Goel, Fully integrated, automated, and smartphone enabled point-of-source portable platform with microfluidic device for nitrite detection, *IEEE Trans. Biomed. Circuits Syst.* 13 (2019) 1518–1524, <https://doi.org/10.1109/TBCAS.2019.2939658>.
- [132] J.H. Shin, S. Choi, Open-source and do-it-yourself microfluidics, *Sens. Actuators B Chem.* 347 (2021), 130624, <https://doi.org/10.1016/j.snb.2021.130624>.
- [133] X. Huang, D. Xu, J. Chen, J. Liu, Y. Li, J. Song, X. Ma, J. Guo, Smartphone-based analytical biosensors, *Analyst* 143 (2018) 5339–5351, <https://doi.org/10.1039/c8an01269e>.

**Zhenghua Li** is a postgraduate in the School of Mechanical Engineering at Shenyang Jianzhu University under the supervision of Prof. Wenfeng Liang. His current research focuses on the design, fabrication, and application of microfluidic chip for drug-loading for biomedical and chemical research.

**Baoliang Zhang** is a postgraduate in the School of Mechanical Engineering at Shenyang Jianzhu University under the supervision of Prof. Wenfeng Liang. His current research focuses on the microfluidics mixing and optically induced dielectrophoresis (ODEP).

**Dan Dang** is an Associate Professor in the School of Sciences at Shenyang Jianzhu University. Her research mainly focuses onto micro/nano robotic hydrodynamics.

**Xieliu Yang** is an Associate Professor in the School of Mechanical Engineering at Shenyang Jianzhu University. His research interest lies in computer vision measurement, scene image text detection and recognition and image processing.

**Wenguang Yang** is an Associate Professor in the School of Electromechanical and Automotive Engineering at Yantai University. His research interest lies in flexible electronic device, micro and nano manipulation and 4D printing.

**Dr. Wenfeng Liang**, obtained his B. E. degree in Electrical Engineering and Automation (Honors College) from China Jiliang University in 2008 and his Ph. D. degree in Mechanical Engineering from Shenyang Institute of Automation, Chinese Academy of Sciences, in 2014. After graduation, He became a faculty member in School of Mechanical Engineering of Shenyang Jianzhu University, serving as an Assistant Professor in 2014. Simultaneously, he did Postdoctoral research in the same institute from 2014 to 2017. Funded by China Scholarship Council, he also performed one-year research in Dept. of Mechanical Engineering and Materials Science, Duke University, NC, USA in 2018. Since 2021, he has been promoted as a Full-Professor and selected as a Ph. D. supervisor. He has served as the principal investigator for more than 10 projects funded by a series of agencies involving NSFC. His research interest lies in Microfluidics, AC electrokinetics, Acoustophoresis and BioMEMS/NEMS.